THE ROLE OF PITUITARY ADENYLATE CYCLASE-ACTIVATING POLYPEPTIDE IN SYMPATHETIC REGULATION OF BROWN ADIPOSE TISSUE FUNCTION

by

Md Shajjad Hossain

BSc (Hons.), Jahangirnagar University, 2021

THESIS SUBMITTED IN PARTIAL FULFILLMENT OF
THE REQUIREMENTS FOR THE DEGREE OF
MASTER OF SCIENCE
IN
BIOCHEMISTRY

UNIVERSITY OF NORTHERN BRITISH COLUMBIA

November 2024

ABSTRACT

Obesity is a multi-factorial, chronic metabolic disease that forms due to the imbalance of energy metabolism. Scientists are actively working to identify potential therapeutic targets to combat obesity. Pituitary adenylate cyclase-activating polypeptide (PACAP) has been recognized as a neuropeptide involved in regulating adaptive thermogenesis, a physiological mechanism of energy expenditure. The role of PACAP in catecholamine secretion is well-studied at the sympatho-adrenomedullary axis; however, the function of PACAP in the peripheral sympathetic nervous system (SNS) is not characterized. We developed an *ex vivo* model aiming to study PACAP's role in the peripheral ganglia in regulating catecholamine secretion and downstream adrenergic signaling. To validate the model, we used two nicotinic acetylcholine receptor (nAChR) agonists (dimethylphenylpiperazinium (DMPP), nicotine) to stimulate postganglionic nerves of the stellate ganglia and assessed molecular markers (cyclic adenosine monophosphate (cAMP) and phospho-hormone-sensitive lipase (p-HSL) (Ser563)) of norepinephrine-stimulated adrenergic signaling in interscapular brown adipose tissue (iBAT). Delivering nAChR agonists to the stellate ganglia did not increase the production of cAMP and p-HSL (Ser563) in iBAT, demonstrating that, as currently implemented, our model is not suitable to study PACAP's function in the peripheral ganglia. Although the model was deemed to be unsuccessful, outcomes of this study have helped us understand the challenges of working with a sympathetic ganglion, and the optimization of protocols to measure molecular markers of adrenergic stimulation established in this study will be useful for future studies examining sympathetic nerve activity in peripheral organs.

TABLE OF CONTENTS

LIST OF TABLES

LIST OF FIGURES

LIST OF ABBREVIATIONS

ACh	Acetylcholine
ATP	Adenosine triphosphate
ATGL	Adipose triglyceride lipase
ACTH	Adrenocorticotropic hormone
APS	Ammonium persulfate
ANOVA	Analysis of variance
ARRIVE	Animal Research: Reporting *In Vivo* Experiments
BCA	Bicinchoninic acid
BMI	Body mass index
BSA	Bovine serum albumin
BAT	Brown adipose tissue
CREB	cAMP response element-binding protein
COMT	Catechol O-methyltransferase
CNS	Central nervous system
CRH	Corticotropin-releasing hormone
cAMP	Cyclic adenosine monophosphate
DAG	Diacylglycerol
DHPG	3,4-dihydroxyphenylglycol
DMPP	Dimethylphenylpiperazinium
DOPA	3,4-dihydroxyphenylalanine
DDC	Dopa decarboxylase
DβH	Dopamine β-hydroxylase

ETC	Electron transport chain
ELISA	Enzyme-linked immunosorbent assay
EDTA	Ethylenediaminetetraacetic acid
EPAC	Exchange protein activated by cAMP
FADH	Flavin adenine dinucleotide
FFAs	Free fatty acids
GPCRs	G-protein coupled receptors
HPLC	High performance liquid chromatography
HSL	Hormone-sensitive lipase
HPA	Hypothalamic-pituitary-adrenocortical
IP_3	Inositol triphosphate
iBAT	Interscapular brown adipose tissue
kD	Kilo Dalton
mRNA	Messenger RNA
Mi-CK	Mitochondrial creatine kinase
MAO	Monoamine oxidase
MHPG	3-methoxy-4-hydroxyphenylglycol
NADH	Nicotinamide adenine dinucleotide
nAChR	Nicotinic acetylcholine receptor
NMN	Normetanephrine
OD	Optical density
PNS	Parasympathetic nervous system
PVN	Paraventricular nucleus

PNMT	Phenylethanolamine N-methyltransferase
PBS	Phosphate-buffered saline
PDCC	Phospho-dependent depolarizing cation conductance
PLC	Phospholipase C
p-HSL	Phospho-HSL
PACAP	Pituitary adenylate cyclase-activating polypeptide
pNpp	p-nitrophenyl phosphate
PVDF	Polyvinylidene fluoride
PKA	Protein kinase A
RIPA	Radio-immunoprecipitation assay
SDS	Sodium dodecyl sulfate
SNS	Sympathetic nervous system
TEMED	Tetramethylethylenediamine
CCAC	Canadian Council on Animal Care
TCA	Tricarboxylic acid cycle
TBS	Tris-buffered saline
TH	Tyrosine hydroxylase
UCP1	Uncoupling protein-1
VMA	Vanillylmandelic acid
VIP	Vasoactive intestinal peptide
VMN	Ventromedial nucleus
WAT	White adipose tissue
WHO	World Health Organization

ACKNOWLEDGEMENT

I would like to sincerely acknowledge the financial support I have received from the Natural Science and Engineering Council of Canada (NSERC) and the University of Northern British Columbia throughout my degree period. This financial support helped me focus on my research and dedicate full-time work in the lab to gain knowledge and skills without being tensed for managing living costs. I am genuinely grateful to my supervisor, Dr. Sarah Gray, for her unwavering mental support and direct mentorship, which were badly needed for me as an international student to adapt to a new curriculum. Dr. Gray has taught me how to implement a research idea and be motivated throughout this challenging journey. I joined the lab with bare hands-on experience but with a passion for learning research, and Dr. Gray's supervision helped awaken the hidden research potential in me.

I appreciate Dr. Kendra Furber and Dr. Chow Lee for serving as members of my Graduate Supervisory Committee. I found Dr. Furber and Dr. Lee cooperative in responding to questions related to my research, and their valuable feedback helped move this thesis work forward. I especially thank Dr. Andrew Giles, a member of Gray and Furber's lab, for guiding me to learn the technical and data-analyzing skills required to complete this thesis. I would like to thank Sydney Cruch and Sianne Vatour for taking amazing care of our animal model, and heartfelt thanks to mice for making this research possible.

Lastly, I appreciate Yamna Rahim, the lab manager of Gray lab, for her guidance and assistance during the mice dissection. Thanks to all lab members of the Gray lab for creating a welcoming and friendly environment in the lab, which made the learning process enjoyable.

DEDICATION

I would like to dedicate this thesis to myself for doing hard work to complete an advanced degree using a second language and for surviving in a new country without any loveable person beside.

I dedicate this thesis to my parents, who are my inspiration to keep going forward no matter how challenging the path is. I am grateful to my Dad for all his hard work and sacrifice to fulfill our fundamental needs and gift us a better life. Mom, thank you for being my first tutor, mentor, and friend, and especially thanks for providing mental support during my tough time.

I dedicate this thesis to my beloved graduate supervisor, Dr. Sarah Gray, who provided me the opportunity to work with her and obtain an MSc degree in a North American country, which was one of my long cherished dreams.

Chapter One: Introduction to Endocrine Regulation of Energy Homeostasis

1.1 OBESITY: AN IMPAIRMENT OF ENERGY HOMEOSTASIS

Worldwide, the prevalence of obesity has increased by 28% over the last 30 years and is growing exponentially (Smith and Smith 2016). In the United States, it was found in a 2014 report that a single obese person's health cost was $1,901 per year, making $149.4 billion in health costs at the national level (Chooi, Ding, and Magkos 2019). The estimated annual health cost of obesity in Canada is around $11 billion (Campbell-Scherer and Sharma 2016). The impact of obesity on morbidity, mortality, and health care costs makes it a public health burden with detrimental effects on quality of life and mental health (Upadhyay et al. 2018).

The World Health Organization (WHO) defines overweight and obesity as abnormal or excessive fat accumulation that drives potential health issues (World Health Organization 2015). Body mass index (BMI) is one of several clinical indicators used to assess the presence of obesity. BMI is calculated using a person's height (m) and weight (kg). Having a BMI value of more than 25 kg/m^2 is considered overweight, and greater than 30 kg/m^2 is classified as obese (World Health Organization 2015). Although BMI is used as a measure of obesity, it is not a direct approach to measuring body fat, and there is no linear relationship between the percentage of body fat and BMI (Rothman 2008).

Although there is a misconception that obesity is caused by a lack of an ideal meal plan and physical exercise, it has been experimentally proven that obesity is a multifactorial medical condition influenced by genetic, metabolic, behavioral, social, and environmental aspects (Upadhyay et al. 2018). A proper balance between three biochemical and behavioral processes controls body weight: food intake, energy expenditure, and energy storage (Spiegelman and Flier 2001). It is well-known that the regulation of food uptake depends on

the interaction of a homeostatic component focusing on energy balance and a hedonic component seeking food-associated pleasure (Figure 1.1). While the homeostatic control of food intake relates to adipose and gastrointestinal hormones (e.g., leptin, insulin, ghrelin) that convey the level of energy stores and intake to the brain, the hedonic control of food intake associates with reward mechanisms mediated by neurotransmitters such as dopamine and serotonin (Pinto, Cominetti, and da Cruz 2016).

In a state of positive energy balance, energy consumption (nutrient intake) is higher than energy expenditure (physical exercise, basal metabolic rate, and thermogenesis). In this state, excess energy gets deposited as triglycerides in fat cells (Chooi et al. 2019). This deposition of fat increases the mass and size of fat tissues through the hyperplasia and hypertrophy of fat cells. The expansion of fat tissue (known as adipose tissue) is associated with the development of other diseases, including type 2 diabetes, osteoarthritis, heart disease, and cancer, in part through the development of a pro-inflammatory state that alters adipose tissue function and its communication with the central nervous system (CNS) and other peripheral tissues (Bray 2004). The connection between energy metabolism, adipose tissue dysfunction and metabolic disorders makes adipose tissue a potential target organ for further research in medical science.

1.2 THE ROLE OF ADIPOSE TISSUE IN ENERGY HOMEOSTASIS

Adipose tissue is composed of adipocyte cells, macrophages, endothelial cells, fibroblasts, and collagen (Cinti 2005). One of the major functions of this tissue is to store lipids as an energy reservoir. The plasticity of this tissue makes it a dynamic, metabolically active organ critical for the regulation of energy metabolism, insulin sensitivity, body temperature, and immune responses (Sakers et al. 2022). There are three types of adipocytes-

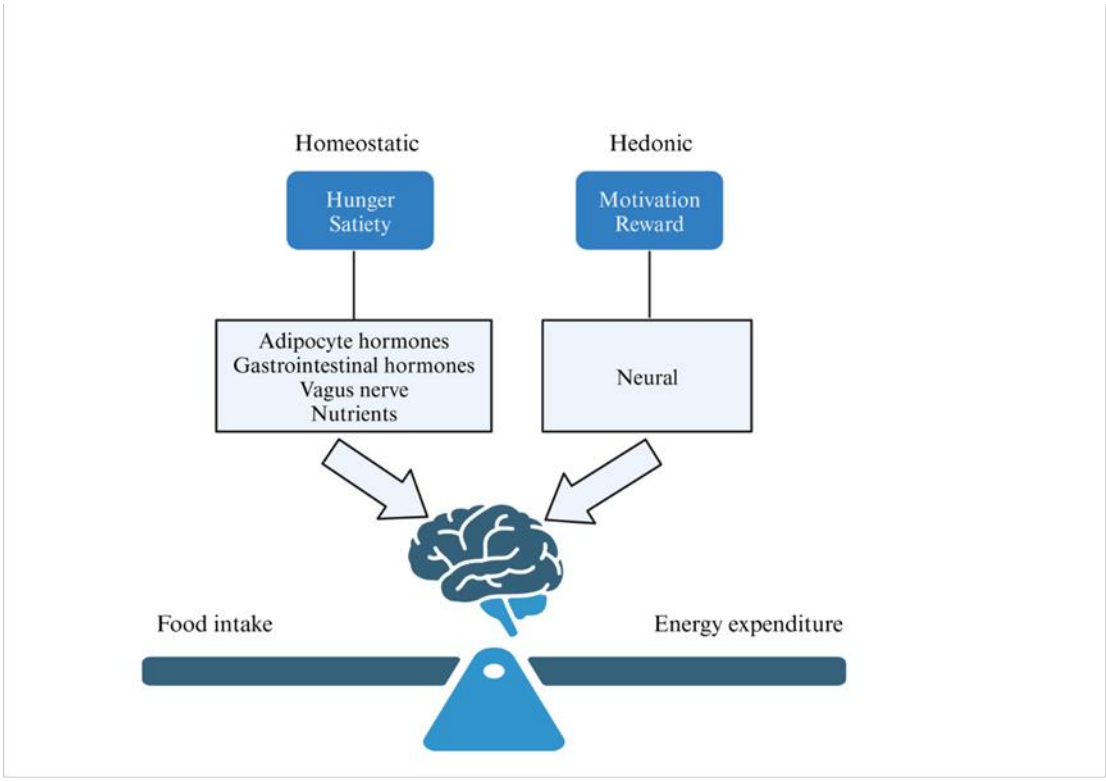

Figure 1.1 Homeostatic and hedonic control of energy balance. The central nervous system (CNS) can contribute to energy homeostasis by regulating the release of hormones and factors involved in food intake and metabolism. The hedonic pathway involves food-associated reward mechanisms. The figure was created with BioRender.com with information from Pinto et al. 2016.

white, beige, and brown (Figure 1.2). White adipocytes are associated with lipid storage and release, and beige and brown adipocytes are the key sites of adaptive thermogenesis, a biochemical process that results in the production of heat in response to thermogenic stimuli such as cold and overfeeding (Chen et al. 2020). WAT stores excess energy for future use in times of nutrient scarcity, but extended fat deposition leads to chronic obesity and contributes to comorbidities, including metabolic disease. The plasticity makes WAT flexible to drive either the storage of energy as triglycerides (lipogenesis) or the release of energy as free fatty acids (lipolysis) based on the organism's energetic needs. For instance, in response to thermogenic stimuli such as a cold environment, the subcutaneous white adipocyte undergoes a 'beiging' or 'browning' process that induces thermogenic pathways to produce heat (Harms and Seale 2013). However, this structural transdifferentiation of subcutaneous white adipocyte is reversed in five weeks of warm adaptation (Rosenwald et al. 2013). Thus, the ability of adipocytes to interconvert from white to beige features is an example of plasticity that is being explored as a therapeutic target to combat obesity by maintaining energy balance.

Adipose tissue is also an endocrine organ, secreting a variety of hormones collectively known as adipokines. Adiponectin and leptin were the first two discovered adipokines that led to the exploration of other adipose-derived hormonal factors (Funcke and Scherer 2019). Both of these adipokines are involved in regulating energy metabolism in the body. Adiponectin can increase fatty acid oxidation and reduce glucose levels by lowering gluconeogenesis in the liver, thus promoting insulin sensitivity (Esteve, Ricart, and Fernández-Real 2009). Leptin, on the other hand, acts in the hypothalamus to communicate the level of energy stores by circulating at levels that relate to the amount of white adipose

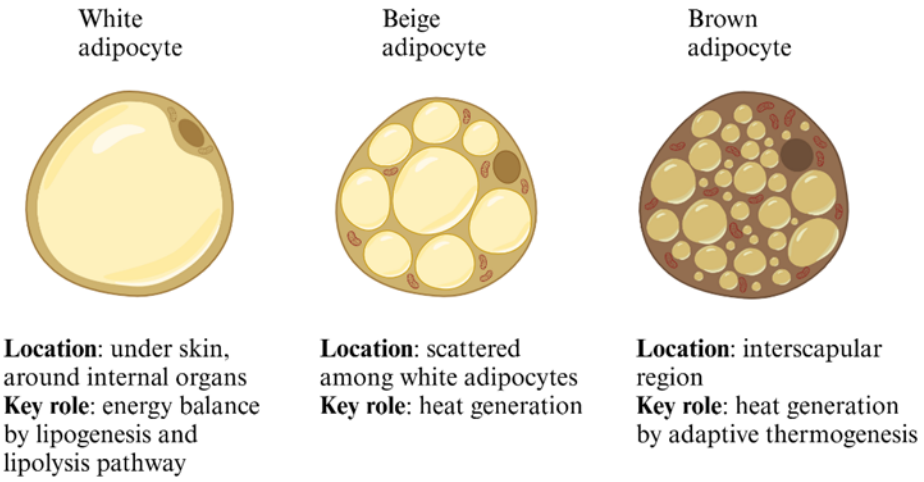

Figure 1.2 Morphology of three adipocytes. White adipocytes have a large lipid droplet which pushes the nucleus to the side of the cell side. Under certain conditions (e.g., cold stress), beige adipocytes differentiate within white adipose tissue depots to support thermogenic capacity. Beige adipocytes contain smaller lipid droplets and more abundant mitochondria than white adipocytes. Brown adipocytes have multilocular lipid droplets and abundant mitochondria that drive adaptive thermogenesis. The figure was created with BioRender.com.

tissue. For example, in a lean state with small amounts of adipose tissue, circulating leptin is present at low levels, stimulating food-seeking behavior and restricting energetically expensive behaviors, such as reproduction. The endocrine role of adipose tissue is thus critical to the control of energy homeostasis (Pan and Myers 2018).

The classical brown adipocyte is found at the interscapular region and is called the interscapular brown adipose tissue (iBAT). Recent experiments have shown that human brown adipocytes are functionally similar to beige adipocytes in mice (Wu et al. 2012). Brown adipose tissue (BAT) is rich in mitochondria and proteins, making it structurally distinguishable from WAT (Figure 1.2). BAT is a specialized tissue famous for being able to conduct adaptive thermogenesis, a process initiated to maintain body temperature in response to thermogenic stimuli (e.g., cold, overfeeding). These stress conditions stimulate the sympathetic nervous system (SNS) to release norepinephrine from the postganglionic nerve terminal, which initiates lipolysis in BAT and produces heat (Cannon and Nedergaard 2004) (Figure 1.3). BAT's ability to produce heat from oxidative metabolism in response to thermogenic stimuli is due to the expression of a specialized mitochondrial protein, uncoupling protein-1 (UCP1). This thermogenic feature makes BAT a potential organ that can counteract obesity by burning calories.

1.3 ADAPTIVE THERMOGENESIS IN BROWN ADIPOSE TISSUE

Adaptive or non-shivering thermogenesis is a regulated heat production process induced in BAT under cold stress conditions. A persistent cold stimulus that will threaten the maintenance of body temperature is detected, integrated at the level of the hypothalamus, and the SNS is activated. Norepinephrine is secreted from sympathetic nerve endings innervating BAT, which binds with adrenergic receptors located on brown adipocytes. Although

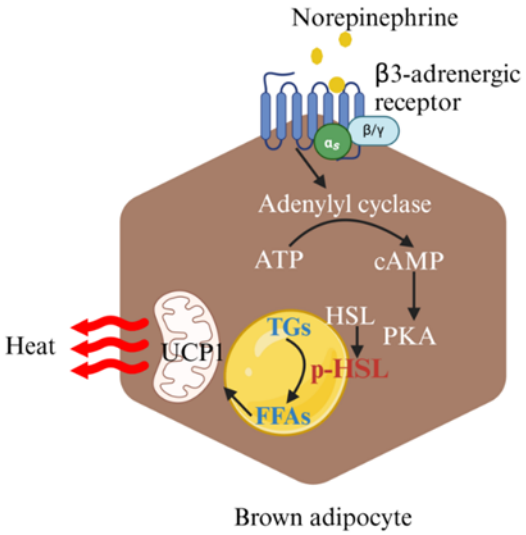

Figure 1.3 Adaptive thermogenesis process in brown adipose tissue (BAT). Norepinephrine binding turns on downstream signaling in BAT and activates lipolysis. Norepinephrine binding with β3-adrenergic receptor activates adenylyl cyclase, adenylyl cyclase converts adenosine triphosphate (ATP) into cyclic adenosine monophosphate (cAMP), cAMP activates protein kinase A (PKA), PKA phosphorylates and activates hormone-sensitive lipase (HSL) to form phospho-HSL (p-HSL), p-HSL converts triglyceride (TG) into free fatty acids (FFAs), uncoupling protein-1 (UCP1) utilizes FFAs to generate heat by uncoupling ATP synthesis from substrate oxidation. The image was created with BioRender.com with information from Rudecki and Gray 2016.

norepinephrine can bind with all three types of adrenergic receptors (α1, α2, and β), β-adrenergic, specifically β3, stimulation of thermogenesis is well-established (Cannon and Nedergaard 2004). The elevated level of stored fat found in β3-adrenergic-receptor null mice also supports the role of the β3-adrenergic receptor in energy expenditure (Susulic et al. 1995). The β3-adrenergic stimulation activates adenylyl cyclase to generate cyclic adenosine monophosphate (cAMP). cAMP then stimulates protein kinase A (PKA) to phosphorylate hormone-sensitive lipase (HSL) to form the activated phospho-HSL (p-HSL). p-HSL catalyzes the second step of the lipolysis reaction to liberate free fatty acids (FFAs) from triglycerides (Duncan et al. 2007) (Figure 1.3). These FFAs work as a primary energy source for thermogenesis and eventually activate UCP1-mediated proton flux (Cannon and Nedergaard 2004).

BAT mitochondria are rich with UCP1, which maximizes the inner membrane proton conductance capacity and diffuses the proton gradient independently from adenosine triphosphate (ATP) production, leading to heat generation (Cannon and Nedergaard 2004). FFAs released by lipolysis are transferred into mitochondria through the carnitine transporter and converted into acyl CoA by enzymes. Acyl CoA is then β-oxidized and entered in the tricarboxylic acid cycle (TCA) cycle to produce the electron carriers: nicotinamide adenine dinucleotide (NADH) and flavin adenine dinucleotide (FADH). The NADH and FADH molecules are oxidized by the electron transport chain (ETC), which results in the pumping out of protons from the mitochondrial matrix and the generation of proton-motive force. Unlike typical mitochondrial energy production (ATP synthesis), UCP1 utilizes this proton-motive force to drive protons from the intermembrane space to the mitochondrial matrix, thus uncoupling the TCA and oxidative phosphorylation by the ETC from ATP production. The

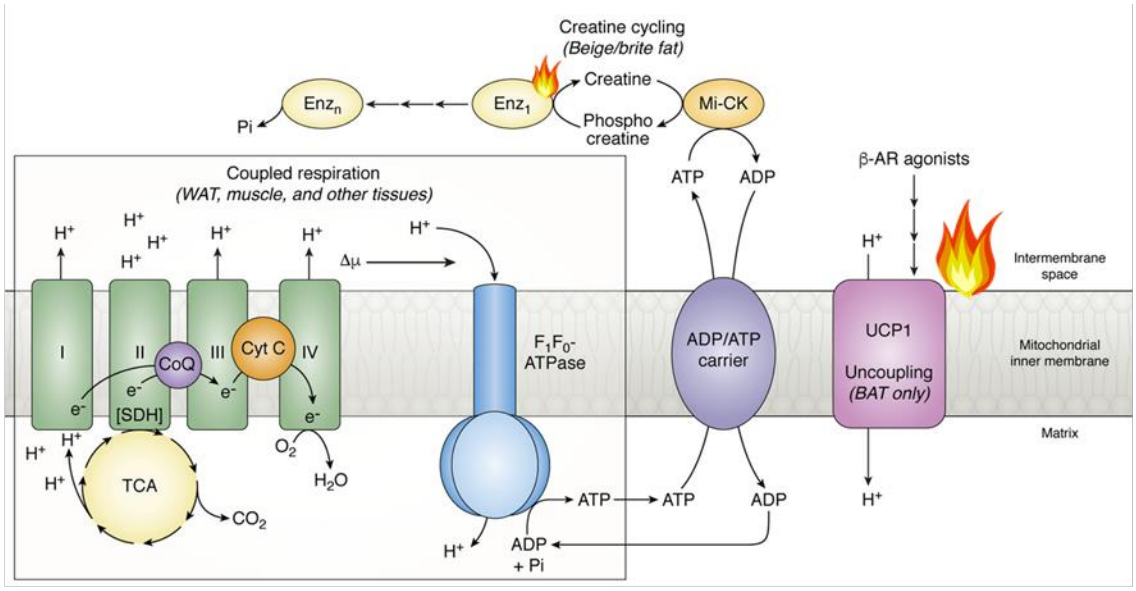

Figure 1.4 Molecular mechanisms underlying adaptive cellular thermogenesis. Coupled respiration is involved in typical energy production by the citric acid cycle (TCA) and the electron transport chain (ETC), resulting in the generation of ATP from substrate oxidation. In brown adipocytes, the thermogenic protein, uncoupling protein 1 (UCP1) can uncouple oxidative phosphorylation and ATP synthesis, resulting in the generation of heat rather than ATP. Creatine cycling is an alternative way of producing heat in beige fat. The thermogenic hydrolysis of ETC-generated ATP fuels the creatine cycle to make phosphocreatine, which is then hydrolyzed by multiple enzymes to generate heat. The figure was taken from Chen et al. 2020 with permission from Elsevier.

proton-motive force energy is dissipated as heat through this UCP1-mediated proton leak process (Cannon and Nedergaard 2004) (Figure 1.4).

Another well-studied mechanism of thermogenesis is the futile cycling of mitochondrial substrates in beige adipocytes, where creatine leads to futile cycling by increasing ADP-dependent respiration. In beige fat, the classic adaptive thermogenic pathway described above exists (Cannon and Nedergaard 2004). In addition, heat is produced due to the coupling of mitochondrial creatine kinase (Mi-CK) to oxidative phosphorylation by the ADP/ATP carrier (Chen et al. 2020) (Figure 1.4). Kazak (2015) has demonstrated that cold exposure can trigger Mi-CK activity to induce creatine metabolism in beige fat. When the endogenous creatine level was reduced in UCP1-deficient mice, the body temperature was found to be significantly lower compared to the UCP1-deficient control group, suggesting the participation of creatine in the thermogenesis process. They also showed that the expression of genes involved in creatine metabolism was induced in UCP1-deficient mice as a compensatory mechanism for lack of UCP-1-dependent thermogenesis, supporting the involvement of creatine metabolism futile cycle in thermal homeostasis (Kazak et al. 2015).

Impairment of energy homeostasis triggers the neuroendocrine and autonomic stress systems, such as the SNS, to activate metabolic processes that will assist in balancing energy levels. Adaptive thermogenesis is one of these metabolic processes activated through the SNS under cold stress.

1.4 SYMPATHETIC REGULATION OF CATECHOLAMINE SECRETION

The SNS is part of the autonomic branch of the peripheral nervous system that responds to “fight-or-flight” conditions. Besides the hypothalamic-pituitary-adrenocortical (HPA) axis, the SNS is a well-known stress-response pathway, which includes the sympatho-

adrenomedullary axis, to respond to different stressors (Goldstein and Kopin 2018). The target tissue of the SNS receives the stress signal from the CNS via neural tracts composed of preganglionic and postganglionic neurons. It is well-established that the SNS is involved in regulating WAT and BAT functions, lipolysis and adaptive thermogenesis, respectively, and these SNS-innervating tissues communicate with the CNS via sensory neurons (Vaughan 2014).

According to the "homeostat" theory, "stress is defined as a situation when a comparator senses a discrepancy between sensed afferent input and a response algorithm, resulting in an altered effector outflow" (Goldstein 2021). Stressors can be categorized as psychogenic and systemic stressors. While psychogenic stressors are consciously processed by the brain, such as work-related stress, systemic stressors are related to physiological stress, such as body temperature change, and are unconsciously processed by the brain (Mustafa 2013). The HPA and SNS axes respond to both systemic and psychogenic stressors and assist in maintaining the body's homeostatic condition (Figure 1.5). The sympatho-adrenomedullary axis responds to stressors by increasing the secretion of catecholamine from the adrenal medulla (Rhoades and Bell 2013) (Ulrich-Lai and Herman 2009) (Figure 1.5).

The postganglionic sympathetic nerves and the chromaffin cells of the adrenal medulla are the key sources of catecholamine in the body (Lymperopoulos, Brill, and McCrink 2016). The sympatho-adrenomedullary axis contains the greater splanchnic nerve, which innervates the adrenal medulla. Under a stress condition, either psychogenic or systemic, the splanchnic nerve works as a preganglionic neuron and secretes neurotransmitters, such as acetylcholine (ACh). The chromaffin cells of the adrenal medulla hold receptors for binding with secreted neurotransmitters, working as a postganglionic

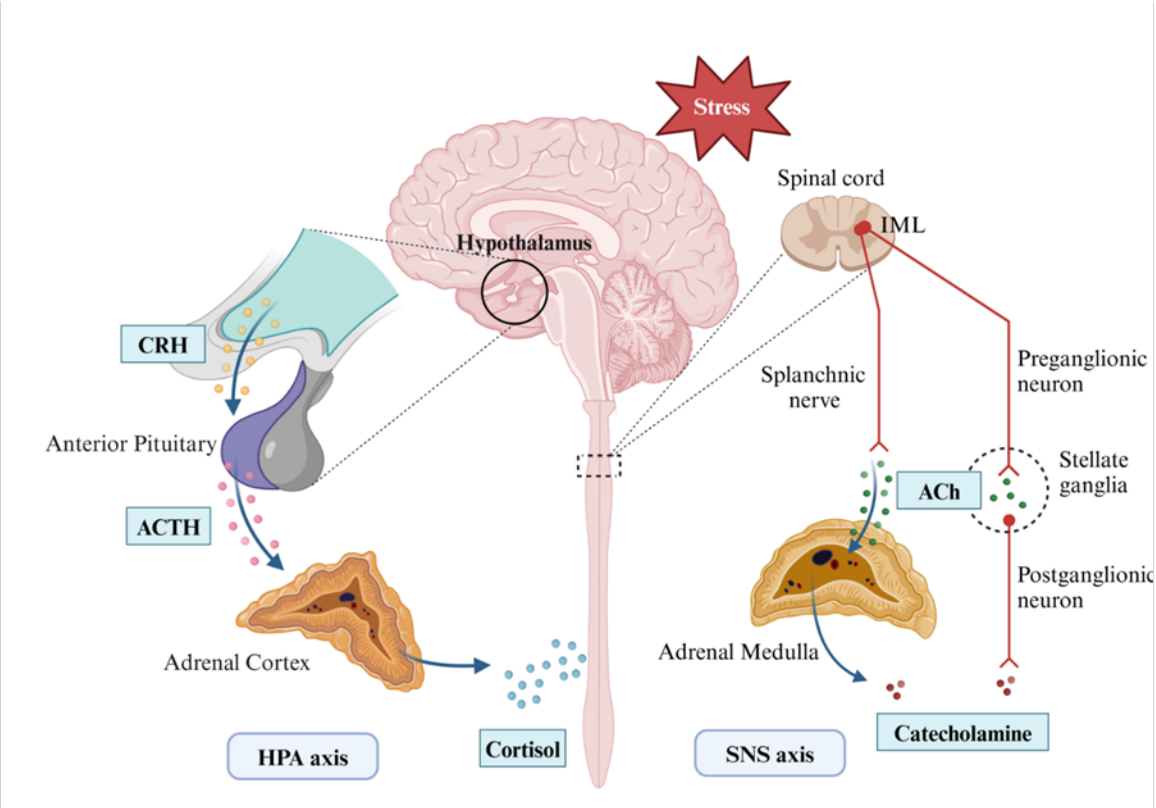

Figure 1.5 An illustration of two major stress-responsive pathways in the body. In the hypothalamic-pituitary-adrenocortical (HPA) axis, stressors stimulate the secretion of corticotropin-releasing hormone (CRH), which heads towards the anterior pituitary and triggers to release the adrenocorticotropic hormone (ACTH). ACTH reaches the adrenal cortex via the bloodstream and instigates the release of cortisol. In the sympathetic nervous system (SNS) axis, stressors stimulate the hypothalamus to send a neuronal signaling cascade to release acetylcholine (ACh) from the splanchnic and preganglionic nerves originating from the intermediolateral nucleus (IML), which triggers the adrenal medulla and postganglionic neuron to secrete catecholamines. The image was created with BioRender.com with information from Rhoades and Bell 2013, Ulrich-Lai and Herman 2009.

neuron. This ligand and receptor binding trigger the chromaffin cells to synthesize and release catecholamines, particularly epinephrine and norepinephrine (Figure 1.6). The released catecholamines reach the targeted organs via the portal system and influence metabolic activities to cope with stressful conditions (Eiden et al. 2018; Lymperopoulos et al. 2016).

The participation of the peripheral SNS in catecholamine synthesis is supported by finding a high expression of tyrosine hydroxylase (TH), a rate-limiting enzyme of catecholamine synthesis, at postganglionic neurons of several peripheral ganglia, including superior cervical ganglia and stellate ganglia (Horwitz and Perlman 1984; Mackay and Iversen 1972). The superior cervical ganglia contain preganglionic projection neurons from the thoracic spinal cord (T1-4) and postganglionic sympathetic neurons that innervate to organs of the head and neck regions (Beaudet, Braas, and May 1998). The stellate ganglion is another peripheral ganglia, and its postganglionic neurons were found to innervate the BAT (François et al. 2019). While the presence of cholinergic and non-cholinergic signaling involved in catecholamine release has been identified in both ganglia, the experimental evidence of catecholamine assessment in peripheral ganglia is not available in the literature.

1.5 CATECHOLAMINE SYNTHESIS AND TURNOVER

Catecholamines consist of three neurotransmitters and hormones named dopamine, epinephrine, and norepinephrine, derived from 3,4-dihydroxyphenylalanine (DOPA), a catecholic amino acid and precursor of catecholamine synthesis. The biosynthesis starts with taking the tyrosine amino acid in the sympathetic neuronal cytoplasm, where the amino acid converts into DOPA catalyzed by TH. DOPA, located in the axonal cytoplasm, is then converted into dopamine by the dopa decarboxylase (DDC) enzyme. Dopamine can now

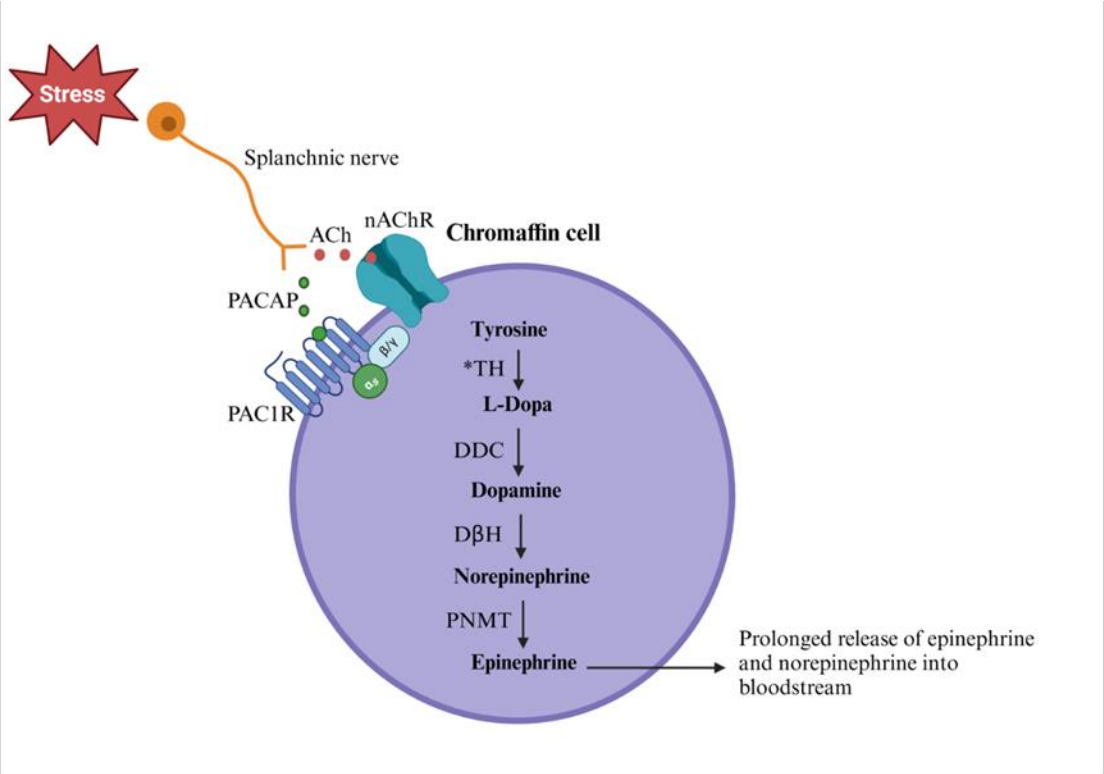

Figure 1.6 A schematic of the sympatho-adrenomedullary axis under stress conditions. Stressors stimulate the greater splanchnic nerve to release acetylcholine (ACh) and PACAP, which bind with the nicotinic acetylcholine receptor (nAChR) and the PACAP-specific receptor (PAC1), respectively located on chromaffin cells. The activation of chromaffin cells causes catecholamine synthesis and release. Tyrosine, the precursor of catecholamine synthesis, is converted into L-Dopa by the rate-limiting enzyme (*) tyrosine hydroxylase (TH). Dopa decarboxylase (DDC) converts L-Dopa into dopamine, dopamine β-hydroxylase (DβH) converts dopamine into norepinephrine, and phenylethanolamine N-methyltransferase (PNMT) converts norepinephrine into epinephrine. The figure was created with BioRender.com with information from Eiden et al. 2018.

shift from the cytoplasm to the vesicle, where the dopamine β-hydroxylase (DβH) enzyme is present to convert dopamine into norepinephrine. The produced norepinephrine can be stored in the vesicle, leaked into the cytoplasm, or released into the synapse (Kgedal and Goldstein 1988) (Figure 1.7).

Catecholamines maintain a dynamic equilibrium by having a constant level in vesicular stores and in the cytoplasm surrounding the vesicle (Figure 1.7). The outward leakage of catecholamine from vesicular stores is balanced by inward active transport through monoamine transporters, allowing a state of equilibrium. Catecholamine turnover is the amount of catecholamine being metabolized and the release of catecholamine into the bloodstream. Although catecholamines can be metabolized in the neuronal cytoplasm after leakage and in the bloodstream after release, it has been identified that 75% of norepinephrine metabolizes intraneuronally (Eisenhofer, Kopin, and Goldstein 2004). It is also well-established that the metabolism of neuronal catecholamine occurs in the nerve cell where the amines are synthesized. The exocytotic release of catecholamine is a part of catecholamine turnover, which can be adjusted by neuronal reuptake and vesicular sequestration (Eisenhofer et al. 2004).

The first step of catecholamine metabolism is oxidative deamination by the monoamine oxidase (MAO) enzyme located in the mitochondrial outer membrane. This deamination process produces a deaminated aldehyde, which is then reduced by aldehyde reductase to form alcohol or acid-deaminated metabolites. It is now well-known that 3,4-dihydroxyphenylglycol (DHPG) is the main metabolic product of norepinephrine deamination, and the plasma level of DHPG refers to the intraneuronal disposition of norepinephrine. DHPG is then catalyzed by the catechol O-methyltransferase (COMT)

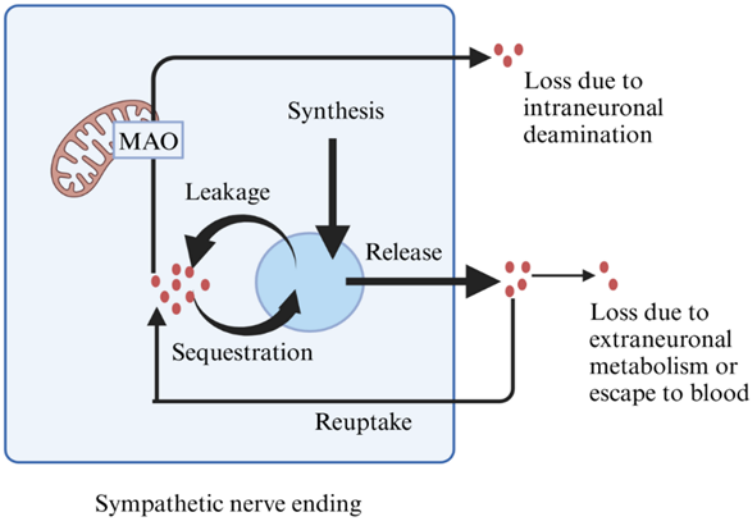

Figure 1.7 An illustration of the vesicular-axoplasmic monoamine exchange process involved in catecholamine metabolism and turnover. Catecholamine turnover, losing catecholamine through metabolism or escaping into the bloodstream, must be replenished by synthesizing more catecholamine to keep the catecholamine levels constant within vesicular stores. The exocytotic release of catecholamine is counter-balanced by neuronal reuptake and vesicular sequestration. The level of vesicular leakage of catecholamines is significant compared to the exocytotic release, meaning intraneuronal metabolism contributes more to the catecholamine turnover. The figure was published in Eisenhofer et al. 2004 and re-created with BioRender.com with permission from Pharmacological Reviews.

enzyme and produces 3-methoxy-4-hydroxyphenylglycol (MHPG). MHPG is eventually converted into vanillylmandelic acid (VMA), the main end-product of norepinephrine metabolism. Norepinephrine can also be metabolized by following the extraneuronal pathway, a minor pathway where norepinephrine is catalyzed by COMT and generates normetanephrine (NMN), which then goes through the oxidative deamination steps to produce VMA (Eisenhofer et al. 2004).

In addition to ACh, researchers have identified that a novel neuropeptide named pituitary adenylate cyclase-activating polypeptide (PACAP) acts as a co-transmitter with the classical neurotransmitter ACh to induce synthesis and prolonged secretion of catecholamines under chronic stress conditions (Eiden et al. 2018; Stroth et al. 2013) (Figure 1.6).

1.6 PITUITARY ADENYLATE CYCLASE-ACTIVATING POLYPEPTIDE

PACAP is a novel neuropeptide first identified in anterior pituitary cell cultures (Miyata et al. 1989). This neuropeptide was named based on its ability to activate adenylyl cyclase, which increases cAMP production. The highly conserved amino acid sequence of PACAP across species reflects PACAP's significance in regulating essential biological functions, and this conserved nature makes scientists interested in doing further research on it (Vaudry et al. 2009). PACAP belongs to the glucagon/secretin superfamily, a group of structurally nearly identical peptide hormones. PACAP is encoded by the ADCYAP1 gene and translated as a 176aa precursor, which is then spliced into the mature PACAP peptide (Vaudry et al. 2009). The most common forms of PACAP present in vertebrates are PACAP-38 and the C-terminally truncated PACAP-27 (Sherwood, Krueckl, and Mcrory 2000).

PACAP has been identified in both the CNS and peripheral nervous system and associated tissues. In the CNS, PACAP has been identified in the brainstem nuclei, hypothalamic nuclei, thalamic nuclei, cerebral cortex, medulla oblongata, posterior pituitary and other regions (Arimura et al. 1991). PACAP is found at the highest levels in the hypothalamus, particularly in the paraventricular nucleus (PVN), a region involved in regulating stress-responsive energy homeostasis (Hashimoto et al. 2011). Although PACAP has versatile roles working as a neurotransmitter, neuroprotectant, neuroregulator, and neuromodulator, PACAP's major function is regulating stress (Mustafa 2013). The ability to regulate both stress axes, the HPA and SNS, to respond to both systemic and psychogenic stress denotes PACAP as a master regulator of stress (Gray and Cline 2019; Mustafa 2013). It was found that the PACAP null mice provided an increased level of corticosterone in plasma under systemic stress but showed a significant drop in corticosterone level under psychogenic stress, stating the role of PACAP in the HPA axis activation to respond to psychogenic stress, but not systemic stress (Lehmann et al. 2013).

PACAP has been identified at the splanchnic adrenomedullary synapse, where PACAP is released from the splanchnic nerve in response to systemic and psychogenic stress (Stroth et al. 2011). PACAP, released from the preganglionic nerve, then binds with receptors on chromaffin cells of the adrenal medulla and regulates the synthesis and secretion of catecholamine. Down-regulation of the messenger RNA (mRNA) level of catecholamine synthesis-related enzymes, TH and phenylethanolamine N-methyltransferase (PNMT), found in PACAP null mice provides insight into the role of PACAP in catecholamine biosynthesis (Stroth et al. 2013). The PACAP antagonist (PACAP 6-38) was able to significantly reduce the catecholamine secretion in adrenal slices, supporting the role of PACAP in catecholamine

secretion (Kuri, Chan, and Smith 2009). The ability of PACAP to induce prolonged secretion of catecholamine came to researchers' attention from the amperometric recording where adding PACAP in ACh-desensitized adrenal slices provided a high spike density (Kuri et al. 2009; Stroth et al. 2013). Besides the splanchnic adrenomedullary synapse, PACAP and its receptors have also been found in superior cervical ganglia and stellate ganglia (Beaudet et al. 1998; Braas and May 1999; Pandher et al. 2023); however, the functional role of PACAP receptors in catecholamine production and release in peripheral ganglia is yet to be determined.

Designing a PACAP null mice model by scientists (Gray et al. 2001; Hamelink et al. 2002) has created opportunities to explore the role of PACAP *in vivo*. Hamelink (2002) used the PACAP null mice strain to show that PACAP is required to balance the plasma glucose levels during hypoglycemic stress (Hamelink et al. 2002). The role of PACAP in adaptive thermogenesis was also established by using the PACAP null mice model, where researchers (Gray et al. 2002) showed the temperature-sensitive phenotype of PACAP null mice with a survival rate of only 11% when raised at 21°C (Gray et al. 2002). The administration of PACAP to the ventromedial nucleus (VMN) of the hypothalamus increased the body temperature and mRNA levels of UCP1 in iBAT, supporting the central thermogenic action of PACAP (Resch et al. 2011). Researchers have recently identified PACAP receptors on BAT (Cline et al. 2019) and on postganglionic nerves of the stellate ganglia (Pandher et al. 2023), which suggests a peripheral role for PACAP in adaptive thermogenesis.

1.7 PACAP RECEPTORS AND RELATED AGONISTS AND ANTAGONISTS

PACAP plays its functional role once it binds with three G-protein coupled receptors (GPCRs) called PAC1, VPAC1, and VPAC2. The mRNA expression of the PAC1 receptor is

profound in the brain, pituitary, and adrenal gland. VPAC1 and VPAC2 are abundant in the lung, liver, and testis (Vaudry et al. 2009). All of these receptors belong to class B GPCRs that bind with PACAP and another structurally similar peptide named vasoactive intestinal peptide (VIP). It has been found that VPAC1 and VPAC2 receptors (type II binding site) have affinity for both PACAP and VIP, whereas the PAC1 receptor (type I binding site) shows high affinity and specificity for PACAP (Harmar et al. 2012; Vaudry et al. 2009). VPAC and PAC receptors have been found to be distributed in central and peripheral nervous systems and associated tissues (Dickson and Finlayson 2009).

The presence of introns in VPAC and PAC receptor genes allows alternative splicing, which produces splice variants that potentially impact the downstream signaling process. The splice variation is well-characterized in the PAC1 receptor with 11 known isoforms in mammals (Dickson and Finlayson 2009). The coding sequences of the N-terminal extracellular domain, transmembrane domain, and intracellular loop of the PAC1 receptor have been found with alternative splicing (Figure 1.8). Alternative splicing in the extracellular N-terminal domain, particularly at exons 3, 4, 5, and 6, produces four isoforms of PAC1 (Harmar et al. 2012). Splicing of exons 4 and 5 (21 amino acids) results in a splice variant called PAC1-short, which was found to have similar affinity for PACAP-38, PACAP-27, and VIP (Dautzenberg et al. 1999). Another PAC1 splice variant is PAC1-very short (PAC1vs) formed by excluding exons 3, 4, and 5 (57 amino acids), and this isoform showed higher affinity for PACAP (PACAP-38> PACAP-27) than VIP, though the affinity was 100 fold lower than the un-spliced PAC1 (Dautzenberg et al. 1999; Pantaloni et al. 1996). The addition of exon 3a (24 amino acids) in between exon 3 and 4 forms another isoform of PAC1 receptor called PAC1-3a found in rats, which showed a reduced affinity to PACAP

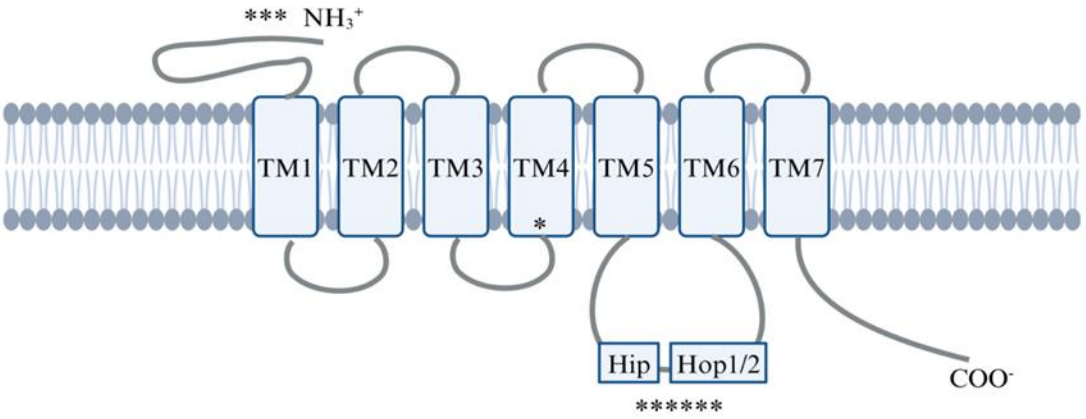

Figure 1.8 An illustration of the PAC1 receptor with its known splice variants. The asterisk (*) sign demonstrates the number of splice variants produced by alternative splicing in the N-terminal extracellular domain, transmembrane domain (TM), and third intracellular loop containing 'hip' and 'hop1/2' exons. The figure was generated with BioRender.com with information from Dickson and Finlayson 2009.

(Daniel et al. 2001). Substitution and deletion of amino acids in the fourth transmembrane domain makes another receptor variant; however, the existence of this variant is not well-established (Dickson and Finlayson 2009). Six splice variants have been found in the third intracellular loop containing hip, hop1, and hop2 exons. The presence of these exons alone or in a combination produces PAC1 variants, such as PAC1-hip, PAC1-hop1, PAC1-hop2, PAC1-hiphop1, and PAC1-hiphop2; however, the PAC1 null variant has no cassette in the third intracellular loop (Dickson and Finlayson 2009). These third intracellular loop splicing variants displayed altered affinity to PACAP and different levels of cAMP and phospholipase C (PLC) production depending on the activation of a specific G protein (G_s and G_q) (Spongier et al. 1993; Yoshimura et al. 1995).

Alternative splicing also produces splice variants in VPAC1 and VPAC2 receptors, but their distribution and functional role still need to be well-studied. Four splice variants have been explored for alternations in amino acid sequence of intracellular domain, transmembrane domain, and C-terminal domain of VPAC1 and VPAC2 receptor genes (Dickson and Finlayson 2009).

Besides PACAP, which acts as an agonist for all three GPCRs, researchers have explored some other VPAC/PAC receptor agonist and antagonist molecules (Table 1.1) that have different specificity for the various receptors. The potency of these natural or synthetic molecules influencing cAMP production or intracellular calcium signaling was used to denote them as an agonist or antagonist of VPAC/PAC receptors (Dickson and Finlayson 2009). Maxadilan, a peptide isolated from the sand fly *Lutzomyia longipalpis* and found to have a different amino acid sequence than PACAP, has been identified as a potent, specific PAC1 receptor agonist; however, the modified version of this peptide named M65 behaves as

Table 1.1 A list of PACAP receptors (PAC1, VPAC1, and VPAC2) agonist and antagonist molecules. '+' sign denotes agonist and '–' sign denotes antagonist property.

Reagents	PAC1	VPAC1	VPAC2
PACAP-38	+	+	+
VIP	Not determined	+	+
Maxadilan	+	Not determined	Not determined
M65	–	Not determined	Not determined
PACAP (6-38)	–	Not determined	Not determined

an antagonist of PAC1 receptor (Moro and Lerner 1997; Uchida et al. 1998). A truncated version of PACAP (PACAP 6-38) acts as an antagonist of the PAC1 receptor for its ability to inhibit cAMP production elevated by PACAP (Leyton et al. 1999).

1.8 THESIS SCOPE AND SIGNIFICANCE

The SNS is well-known for its ability to respond to stress by regulating the secretion of catecholamines, norepinephrine and epinephrine (Rhoades and Bell 2013). It is well-established that the SNS innervates and controls BAT function, with norepinephrine as the key initiating factor for lipolysis and adaptive thermogenesis (Kooijman, van den Heuvel, and Rensen 2015). The temperature-sensitive phenotype of PACAP null mice provides insight into PACAP's role in thermogenesis (Gray et al. 2002). Eiden et al. and Stroth et al. have robustly established that PACAP presents at the splanchnic adrenomedullary synapse and regulates the synthesis and sustained secretion of catecholamine from chromaffin cells of the adrenal medulla (Eiden et al. 2018; Hamelink et al. 2002; Stroth et al. 2011). Besides this splanchnic adrenomedullary synapse, the superior cervical ganglia and stellate ganglia receive PACAP-positive preganglionic neurons, and PAC1/VPAC receptors are expressed on postganglionic neurons (Braas and May 1999; Pandher et al. 2023). However, the functional role of PACAP in catecholamine turnover in the peripheral SNS has not been conclusively determined.

The cell bodies of the postganglionic neurons of the stellate ganglia have been found to express PAC1 and VPAC1 receptors (Pandher et al. 2023), and neural tracing studies have shown iBAT to be innervated by postganglionic neurons originating in the stellate ganglia (François et al. 2019). Therefore, we hypothesize that stimulating the stellate ganglia with PACAP will trigger catecholamine-regulated signaling in downstream brown adipose tissue.

The first step in testing this hypothesis is developing an *ex-vivo* model to deliver PACAP to stellate ganglia. Molecular assessment of the adrenergic signaling stimulation by PACAP will be done focusing on marker molecules involved in the lipolysis process in iBAT, considering lipolysis is a well-established downstream target for measuring adrenergic receptor activation. In the following chapters, I will explain our experimental approach to measure the marker molecules of the adrenergic signaling involved in lipolysis. The results of these experiments will assist in understanding the role of PACAP in energy homeostasis by regulating thermogenesis in BAT, proposing PACAP as a therapeutic target to deal with obesity.

Chapter Two: Assessing a New *ex-vivo* Model to Study the Role of PACAP in Catecholamine-induced Adaptive Thermogenesis

2.1 INTRODUCTION

The SNS is a branch of the autonomic nervous system, and its major function is to respond to stress. Stressors activate the SNS to secrete the stress-responsive hormones epinephrine and norepinephrine (Figure 2.1). For instance, hypoglycemia, a systemic stress, activates the SNS to release epinephrine from chromaffin cells of the adrenal medulla that reach adrenergic receptors expressed on cells of the liver via the bloodstream to activate glycogenolysis and gluconeogenesis and restore blood glucose levels to normal levels (Rhoades and Bell 2013). Cold stress is an example of a stressor that stimulates postganglionic neurons of the SNS to release norepinephrine and induce adaptive thermogenesis in adipose tissues, such as iBAT to generate heat to maintain body temperature at 37°C (Cannon and Nedergaard 2004).

The response of SNS to stressors is mediated by ACh neurotransmitter. ACh is a well-known neurotransmitter of the autonomic nervous system that acts as both a first order and second order neurotransmitter to regulate both the SNS and parasympathetic nervous system (PNS). In the SNS, ACh plays its functional role by binding with the nicotinic receptors on postganglionic neurons. In the PNS, ACh binds with the nicotinic receptors on postganglionic neurons and is released from the postganglionic neurons again as a second order neurotransmitter to bind with muscarinic receptors on target tissues (Kandel et al. 2021). Since SNS is the experimental focus of this thesis, I will further describe the ACh-mediated signal transduction in SNS. ACh is secreted from preganglionic sympathetic neurons and binds with nicotinic acetylcholine receptors (nAChR) located on chromaffin cells or postganglionic neurons to regulate epinephrine and norepinephrine secretion, respectively. The nAChR is categorized into two groups based on its primary expression

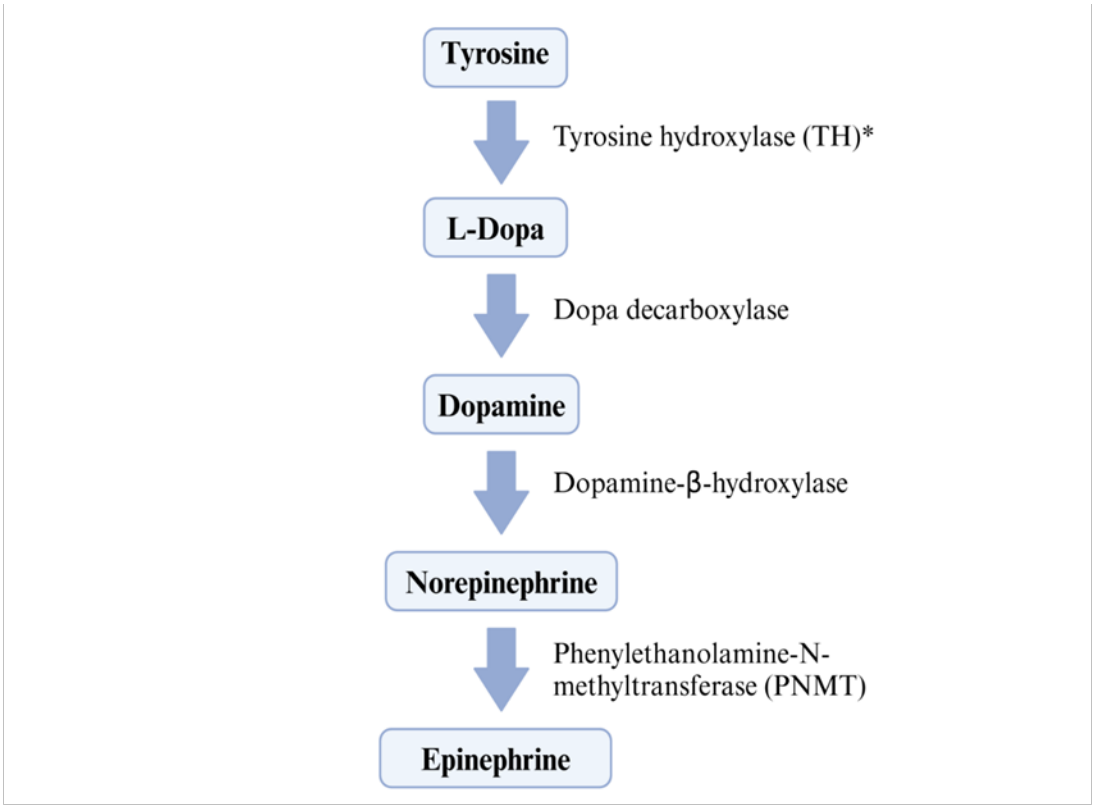

Figure 2.1 The pathway of catecholamine synthesis in chromaffin cells of the adrenal medulla and postganglionic neurons of the sympathetic nervous system. Tyrosine hydroxylase (TH)* is the rate-limiting enzyme of catecholamine synthesis. The diagram was created with BioRender.com.

sites: muscle receptors, which are found at the neuromuscular junction, and neuronal receptors, found throughout the central and peripheral nervous systems. Based on RT-PCR data, twelve receptor subunits (α2-α10 and β2-β4) have been identified to be involved in forming different neuronal nAChR subtypes with a wide range of pharmacological profiles (Hogg, Raggenbass, and Bertrand 2003). For example, the CNS highly expresses α4β2 and α7 subtypes of nAChR, whereas the heteromeric α3β4 subtype is highly expressed in the peripheral SNS and is the key nAChR subtype involved in ganglionic neurotransmission in the autonomic nervous system (Zaveri et al. 2010).

The nAChR is a pentameric receptor and a member of the ligand-gated ion channel superfamily. Each subunit of the nAChR contains an extracellular ligand binding N-terminal domain, a transmembrane domain (TM1-4), an intracellular loop between TM3 and TM4, and a short extracellular C-terminal domain (Hogg et al. 2003). A circular arrangement of five subunits forms a central ion pore. Upon binding of ACh or agonist molecules to the ligand binding site, the nAChR undergoes a conformational change that results in the passage of ions (largely the influx of Na^+ due to the concentration gradient) into the cell through the central pore, thus depolarizing the cell and opening of voltage-gated sodium channels to trigger an action potential (Kandel et al. 2021). The generated action potential induces calcium influx into the cell and mediates the exocytotic release of catecholamine from calcium-dependent large dense-core vesicles (Eiden et al. 2018; Kandel et al. 2021).

Known agonists of nAChR that mimic the function of endogenous ACh by binding with the nAChR include nicotine and dimethylphenylpiperazinium (DMPP) (Haass and Kübler 1997). Binding of these agonists to the nAChR has been shown to mimic the actions of ACh, stimulating the release of catecholamine from peripheral postganglionic nerve

terminal and chromaffin cells of the adrenal medulla (Haass and Kübler 1997). For example, DMPP's ability to stimulate nAChR involved an experiment using isolated, intact superior cervical ganglia incubated with 100 μM DMPP, which resulted in an increased TH and DOPA in culture media, precursor compounds of catecholamine synthesis (Horwitz and Perlman 1984) (Figure 2.1). DMPP's ability to mimic ACh activity was shown with respect to energy expenditure when subcutaneous administration of DMPP to diet-induced obese mice reduced body weight and fat mass along with increased UCP1 expression in BAT (Clemmensen et al. 2018). Nicotine is another well-known nAChR agonist. *In vitro* experiments in primary cultures of chromaffin cells demonstrated nicotine's ability to evoke endogenous catecholamine release by activating the nAChR (Mizobe and Livett 1983). The nicotine-induced catecholamine release was found to be significantly higher in the presence of extracellular Ca^{2+}, demonstrating that calcium promotes the exocytotic release of catecholamine from chromaffin granules. Finding an increased norepinephrine content in iBAT of rats after delivering nicotine subcutaneously also supports the role of nicotine in catecholamine release (Haass and Kübler 1997; Lupien and Bray 1988).

nAChR-mediated catecholamine release is well-established. Finding the expression of PAC1 receptor along with nAChR on chromaffin cells suggested the role of PACAP as a second neurotransmitter in augmenting the cholinergic stimulation of catecholamine production and release (Eiden et al. 2018; Kao et al. 2001). Researchers have demonstrated that PACAP is a neuropeptide that is a co-transmitter with ACh and augments catecholamine release during stress. The inability of ACh alone to restore and maintain blood glucose levels in PACAP null mice following insulin-induced hypoglycemia demonstrated the necessity of PACAP for sustained epinephrine-induced reversal of hypoglycemia (Eiden et al. 2018;

Stroth et al. 2011). The splanchnic adrenomedullary synapse is a well-studied part of the SNS. PACAP and ACh are secreted from the splanchnic nerve and bind with PAC1 receptor and nAChR, respectively, located on the adrenal chromaffin cells to stimulate the catecholamine synthesis and release (Eiden et al. 2018; Stroth et al. 2013) (Figure 1.6). The mechanism of PACAP-induced catecholamine release in chromaffin cells has been reviewed by Eiden (2018) (Figure 2.2). Activation of the PAC1 receptor by PACAP binding activates G_s and G_q proteins, where G_s stimulates cAMP production by adenylyl cyclase and G_q activates PLC beta (PLCβ) to catalyze the conversion of phosphatidylinositol 4,5-bisphosphate into IP_3 and diacylglycerol (DAG). cAMP produced by G_s activates exchange protein activated by cAMP (EPAC), a guanine nucleotide exchange factor, which stimulates PLC epsilon (PLCƐ) catalysis and forms IP_3 and DAG. IP_3 mediates the exocytotic release of Ca^{2+} from the endoplasmic reticulum through the IP_3 receptor, which results in increased intracellular Ca^{2+} ions necessary for the exocytotic release of catecholamine. DAG and released Ca^{2+} activate protein kinase C, which phosphorylates and activates phospho-dependent depolarizing cation conductance (PDCC), an ion channel required for voltage-gated calcium channel activation and secretion of catecholamine by PACAP signaling. The calcium channels activated by PDCC augment calcium influx and calcium-dependent exocytotic release of catecholamine from chromaffin granules (Eiden et al. 2018; Tanaka et al. 1996) (Figure 2.2).

Besides the chromaffin cells of the adrenal medulla, postganglionic neurons of several sympathetic ganglia have been found to express PACAP receptors, including the superior cervical ganglia and the stellate ganglia (Braas and May 1999; Pandher et al. 2023).

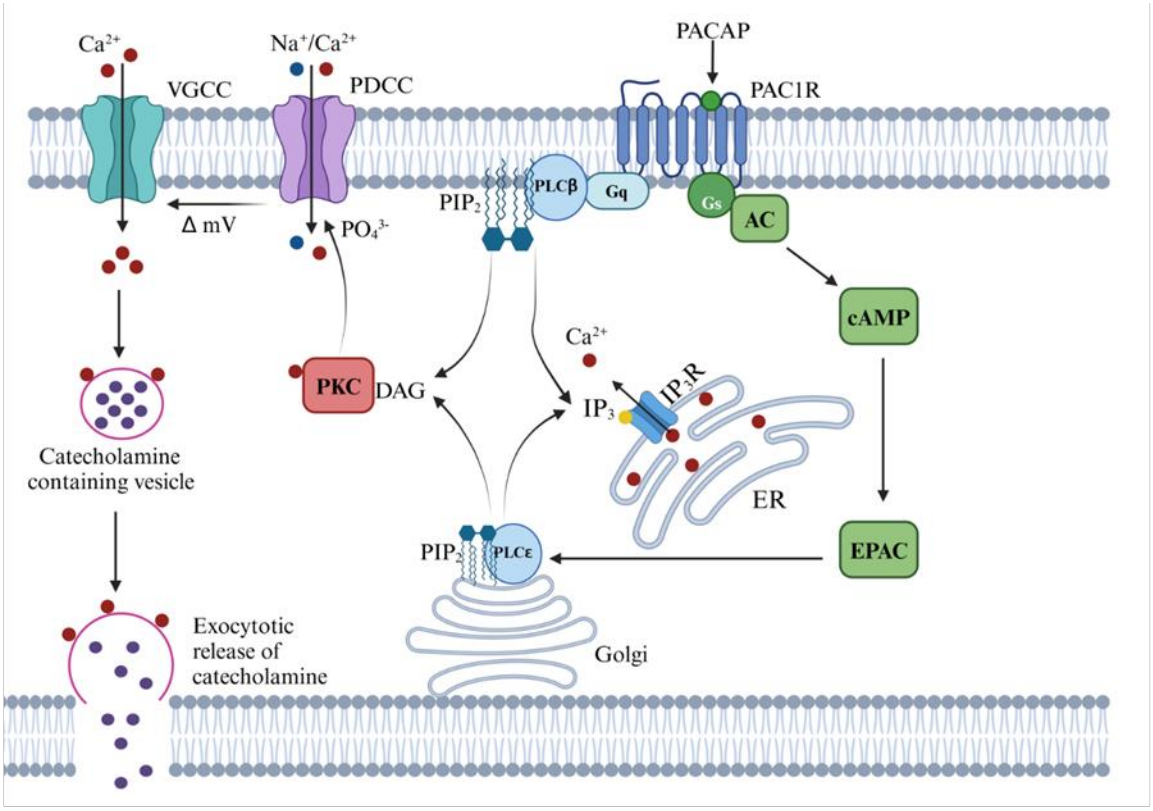

Figure 2.2 A schematic diagram of catecholamine release induced by PACAP signaling. PACAP binding with PAC1 receptor activates G proteins (Gs and Gq). Gs stimulates adenylyl cyclase (AC) to produce cAMP, cAMP activates exchange protein activated by cAMP (EPAC) to stimulate phospholipase C epsilon (PLCƐ). Gq protein stimulates PLC beta (PLCβ). PLC catalyzes phosphatidylinositol 4,5-bisphosphate (PIP2) conversion into inositol triphosphate (IP_3) and diacylglycerol (DAG). IP_3 binds with IP_3 receptor and mediates Ca^{2+} ion release from the endoplasmic reticulum (ER). DAG and Ca^{2+} activate protein kinase C (PKC), which phosphorylates phospho-dependent depolarizing cation conductance (PDCC) channel to activate voltage-gated calcium channels (VGCCs). Activated VGCCs augment calcium influx and calcium-dependent exocytotic release of catecholamine from chromaffin granules. The image was created with BioRender.com with information from Eiden et al. 2018.

This has prompted scientists to explore the role of PACAP receptors in catecholamine synthesis and release in postganglionic neurons originating from peripheral ganglia. While epinephrine is the final end-product of catecholamine synthesis occurring in the chromaffin cells of the adrenal medulla (Figure 2.1), norepinephrine is the primary neurotransmitter released by the postganglionic neuron of peripheral sympathetic ganglia to activate SNS-innervated organs, such as BAT (Eiden et al. 2018). Interestingly, release of catecholamines from the adrenal medulla and peripheral sympathetic ganglia is stressor-specific, and the inter-relationship between these stress-responsive pathways was analyzed by plasma epinephrine and norepinephrine levels (Goldstein and Kopin 2018). For example, hypoglycemia, a metabolic threat, provided a higher epinephrine level in plasma than norepinephrine, indicating the stimulation of the adrenomedullary axis during hypoglycemia. Cold stress, on the other hand, elicited a higher norepinephrine level in plasma compared to epinephrine (Goldstein and Kopin 2018), identifying activation of peripheral sympathetic ganglia during cold stress as the primary signal for initiation of thermogenesis in BAT.

As described in section 1.3 of Chapter 1, adaptive thermogenesis induced in BAT is controlled by norepinephrine secreted from sympathetic nerve terminals. The discovery of the high-density sympathetic nerve fibers in BAT aligns with the important role of the SNS in regulating energy expenditure (Kooijman et al. 2015). Recently, the origins of sympathetic nerve fibres in BAT have been confirmed. François et al. (2019) used pseudorabies virus retrograde tracing to show that iBAT is innervated by postganglionic nerves originating in stellate ganglia and T2-T5 sympathetic chain ganglia (François et al. 2019).

Norepinephrine secreted by postganglionic neurons innervating iBAT binds G-protein coupled β3-adrenergic receptors on brown adipocytes, activating adenylyl cyclase, and

increasing the second messenger cAMP, a classical marker of the β3-adrenergic receptor stimulation (Kandel et al. 2021). Elevated cAMP molecule triggers PKA to phosphorylate cAMP response element-binding protein (CREB), a transcription factor essential for expressing another transcription factor called peroxisome proliferator-activated receptor gamma that increases β-oxidation of fatty acids and expression of the thermogenic protein, UCP1 (Nedergaard, Alexson, and Cannon 1980). PKA also phosphorylates HSL, a 83-kilo Dalton (kD) intracellular lipase that is the rate-limiting enzyme of a three steps reaction converting triacylglycerol to FFAs (Lass et al. 2011). Characterization of HSL null mice that had impaired dyslipidemia due to impaired triacylglycerol hydrolysis, demonstrated the critical role of HSL in regulating lipolysis and energy expenditure (Harada et al. 2003). HSL's catalytic activity is induced by phosphorylation of the protein (p-HSL) (Althaher 2022). The phosphorylated version of HSL (also 83 kD) translocates from the cytosol to the lipid droplet surface, where it associates with adipose triglyceride lipase (ATGL) and other lipase enzymes to mediate triglyceride hydrolysis. *In vitro* peptide mapping studies revealed the primary structure of HSL and identified the PKA-mediated amino acid phosphorylation site of HSL (Ser563) (Belfrage et al. 1997; Garton et al. 1988). Later, Anthonsen (1998) used site-directed mutagenesis to identify two additional phosphorylation sites (Ser659 and Ser660), demonstrating that HSL is subject to complex activity regulation involving multisite phosphorylation (Anthonsen et al. 1998). Measuring the relative expression of p-HSL is a classical target to assess lipolysis induced by β3-adrenergic receptor activation (Arisawa et al. 2024; Cero et al. 2020).

The Gray lab has a long standing interest in studying PACAP's role in thermogenesis. The cold-sensitive phenotype, reduced expression of β3-adrenergic receptor, and low

norepinephrine content in BAT of PACAP null mice demonstrated the role of PACAP in sympathetic regulation of thermogenesis in BAT (Diané et al. 2014; Filatov et al. 2021; Gray et al. 2002). Additionally, given the identification of PACAP receptors (PAC1 and VPAC1) in the stellate ganglia (Pandher et al. 2023), one of the peripheral ganglia from which postganglionic nerves innervating BAT originate (François et al. 2019), I was interested in developing an *ex vivo* model to stimulate the stellate ganglia with PACAP and assess molecular markers of norepinephrine activity (cAMP and p-HSL) to understand if PACAP functions to regulate catecholamine secretion in peripheral sympathetic ganglia. Since the iBAT is innervated by postganglionic neurons originating from the stellate ganglia, we hypothesize that pharmacological stimulation of PACAP receptors on neurons of the stellate ganglia will up-regulate catecholamine release and adrenergic signaling in iBAT, as assessed by the two molecular markers, cAMP and p-HSL (Ser563).

Before working with PACAP, nAChR agonists (DMPP and nicotine) were used as a positive control to validate the approach used to stimulate the stellate ganglia. The method section will describe two approaches to delivering nAChR agonists to the stellate ganglia and optimization of techniques used to measure molecular markers of adrenergic stimulation. The goals for future experiments designed to assess PACAP-mediated stellate ganglia stimulation will be explained in Chapter Three.

The objectives of this chapter are as follows:

AIM 1: Develop an *ex vivo* model using C57BL/6 mice to deliver nAChR agonist to the stellate ganglia to stimulate postganglionic neurons.

AIM 2: Assess downstream adrenergic receptor activation following stimulation of ganglia with nAChR agonist by:

1. Measure the concentration of cAMP using the competitive enzyme-linked immunosorbent assay (ELISA) technique in iBAT collected after delivering nAChR agonist to the stellate ganglia.
2. Measure the ratio of phosphorylated HSL to total HSL using the Western blotting technique in iBAT collected after delivering nAChR agonist to the stellate ganglia.

2.2 MATERIALS AND METHODS

Animals and Experimental Design

Two cohorts of six-week-old wild-type male C57BL/6NCrl (strain code 027) mice were purchased from Charles River Laboratories (Sherbrooke, Quebec, Canada) and kept at the Northern Health Sciences Research Facility for an additional six weeks, so mice were 12 weeks old at the time of experiments. Mice (3-5 per cage) were housed on a HEPA-filtered caging system (APC Filtration Inc., Brantford, Ontario, Canada) with sterile corncob bedding and placed on a 12:12-hour night:light cycle (700-1900h). Mice had *ad libitum* access to rodent chow diet (LabDiet 5001, LabDiet Inc., Brentwood, Leduc, Alberta, Canada; metabolized energy 3.02 kcal/g) and water. The body mass (g) of mice was recorded once a week to socialize mice to be handled and to monitor any potential health declines for stress. Twenty-four hours before dissection, mice were housed in an individual cage with all amenities. On the day of experiments, mice were individually taken to the lab immediately before dissection to minimize environmental stress that can be induced by waiting in the lab. All protocols using animals were approved by the Animal Care and Use Committee at the University of Northern British Columbia in compliance with standards outlined by the Canadian Council on Animal Care (CCAC).

The first cohort of ten mice was categorized into two groups (n=5): DMPP-treated and phosphate-buffered saline (PBS)-treated (vehicle control) and used to test DMPP (100 μM) as a nAChR agonist (positive control) to stimulate postganglionic neurons originating in the stellate ganglia. The second cohort of 28 mice was divided into four groups (n=7): DMPP (100 μM)-treated, nicotine (100 μM)-treated, PBS-treated, untreated and used to test 2 different nAChR agonists, and a modified delivery approach based on feedback from my committee at my second progress report in April 2024. The second cohort included a second agonist, nicotine, to determine which agonist would be most robust in terms of stimulating the nAChR. In addition, an untreated group was added in addition to the vehicle control, to assess whether the technical approach was influencing the ganglia stimulation.

Ganglia Stimulation and Tissue Collection

First cohort: Mice were euthanized with an intraperitoneal injection of Euthanyl (2000 mg/kg, approximately 0.25 mL). Blood (approximately 0.7 mL) was collected via cardiac puncture to reduce blood release during the dissection of mice, giving a better visualization of the stellate ganglia. The skin on the ventral surface was removed carefully, keeping the neural contact with iBAT intact. The stellate ganglia are located in line with the neck of the first rib, inferior to the subclavian vein, posterior to the medial edge of the superior subclavian artery (Gray 2008; Pandher et al. 2023), and these anatomical landmarks were used to identify the stellate ganglia (Figure 2.3). Mice and dissection tools were placed on a thermal pad (37°C) to avoid cold stimulation of nerves throughout the dissection. 1 μL of 100 μM DMPP solution (catalog no. D5891, Sigma Aldrich, St. Louis, Missouri, United States) heated at 37°C was dropped on each ganglion using a P10 pipette and the solution was allowed to incubate for 3 minutes before collecting the iBAT. PBS (catalog no. D8537,

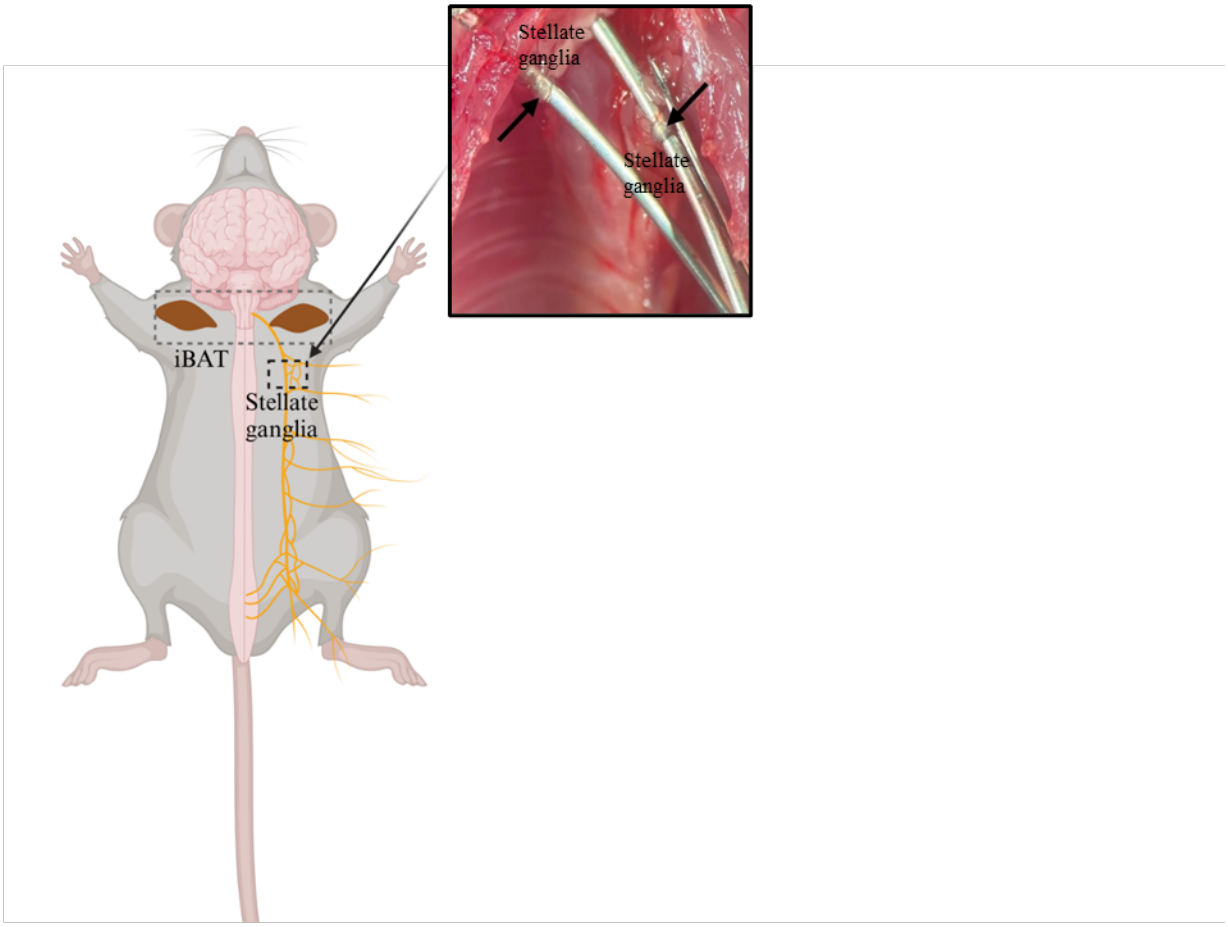

Figure 2.3 The location of stellate ganglia in mouse. The image was captured during dissection and exposure of the ganglia. The mouse schematic was created with BioRender.com.

Sigma Aldrich, St. Louis, Missouri, United States) (vehicle control) heated at 37°C was delivered to ganglia in the same way. The timing from starting the dissection to collecting the iBAT, including the post-administration interval, was 14.3±1.8 minutes. Collected iBAT was stored at -80°C.

Second cohort: Three mice dissecting steps were changed for this cohort to expect a better stimulation of the stellate ganglia: 1. mice were euthanized with diluted pentobarbital (800 mg/kg, approximately 0.2 mL) as per the recommended dose in the euthanasia reference manual; 2. A new nAChR agonist, 100 µM nicotine solution (catalog no. N3876, Sigma Aldrich, St. Louis, Missouri, United States), was used to stimulate the stellate ganglia; 3. 37°C heated PBS, DMPP, and nicotine solutions were injected into the stellate ganglia of the designated group's mice using a syringe with a 32G needle. An untreated group was added to this cohort, where the iBAT was directly collected without touching the stellate ganglia to avoid neuronal firing by dissecting tools. The timing from starting the dissection to collecting the iBAT, including 3 minutes post-administration interval, was 15.1±3.1 minutes, except for the untreated group, where the timing was 1.8±1.2 minutes.

Protein Extraction and Concentration for Western blotting

iBAT collected from both cohorts of mice were processed in a similar way to extract proteins. Half of the iBAT lobe was used to extract proteins for Western blotting, and the remaining half of the lobe was used for the cAMP assay. The frozen iBAT was ground with an individual mortar and pestle for each group in the presence of liquid nitrogen, and the powdered tissue was solubilized in the protein-extracting solvent. Five hundred µL of the radio-immunoprecipitation assay (RIPA) lysis and extraction buffer (catalog no. 89900, ThermoFisher Scientific, Waltham, Massachusetts, United States) prepared with halt™

protease and phosphatase inhibitor cocktail (100X) and 0.5M ethylenediaminetetraacetic acid (EDTA) (100X) (catalog no. 78440, ThermoFisher Scientific, Waltham, Massachusetts, United States) was used to extract protein for Western blotting. The tissue lysates were centrifuged at 14,000 x g for 15 minutes, and the supernatant was transferred into a new eppendorf tube.

The protein concentration of supernatants was quantified using the bicinchoninic acid (BCA) assay kit (catalog no. 23227, ThermoFisher Scientific, Waltham, Massachusetts, United States). The supernatant was further diluted (1:5) in the protein-extracting solvent. A serial dilution of bovine serum albumin (BSA) ranging from 2,000 µg/mL to 0 µg/mL was used to prepare the standards for the BCA assay. Twenty five µl of each standard (triplicate) and diluted sample (individual) were loaded into a 96-well plate, followed by adding 200 µl of working solution in each well. The plate was then incubated at 37°C for 30 minutes. After the incubation, the plate was placed in the BioTek Synergy Neo2 microplate reader (Agilent, Santa Clara, California, United States) to read the absorbance at 562 nm. The average net optical density (OD) for each standard and sample was calculated by subtracting the average absorbance of the blank. Protein concentration (µg/mL) of samples was determined by plotting the net OD values in the standard curve (GraphPad Software, version 9 for Macintosh, San Diego, California, United States).

Tissue Extraction for cAMP assay

The remaining half lobe of the iBAT was ground with an individual mortar and pestle for each group in the presence of liquid nitrogen, and the powdered tissue was dissolved in ten volumes of 0.1M HCl (catalog no. ab290713, Abcam, Cambridge, United Kingdom) to extract cAMP molecule and proteins. The tissue lysates were centrifuged at 14,000 x g for 15

minutes, and the supernatant was transferred into a new eppendorf tube. The protein concentration of supernatants quantified by following the BCA assay protocol described above was used to normalize the cAMP concentration (pmol cAMP/mg protein) as per the manufacturer's instructions.

cAMP assay

The intracellular cAMP in iBAT was quantified using the colorimetric competitive immunoassay kit (catalog no. ab290713, Abcam, Cambridge, United Kingdom, intra-assay CV=4.09% and inter-assay CV=18.69% for 2 pmol/mL, minimum detection limit=0.006 pmol/mL). Before working with samples from the first cohort, an optimized protocol was established following the acetylated format and using different dilution factors (1:3, 1:5) for samples. The optimized protocol described below was used for both cohorts' samples to assess the cAMP concentration.

The tissue lysates were further diluted (1:5) in 0.1M HCl. The 2,000 pmol/mL stock standard solution was used to prepare 20 pmol/mL standard 1, and the remaining four standards were prepared using serial dilution of standard 1 in 0.1M HCl. The acetylating reagent prepared by mixing acetic anhydride and triethylamine (1:2) was added to diluted samples and standards to increase the sensitivity of the assay.

The anti-rabbit antibody (secondary antibody) coated 96-well plate was used to run the assay. Since 0.1M HCl was used as the diluent, the neutralizing reagent was loaded into wells. One hundred µl of each standard (triplicate) and diluted sample (individual) were loaded into the appropriate wells. Fifty µl of alkaline phosphatase conjugated-cAMP antigen and cAMP-specific rabbit antibody (primary antibody) were aliquoted to wells, respectively, making a competition between the alkaline phosphatase conjugated-cAMP and cAMP in

tissue lysates to bind with the cAMP-specific antibody. The plate was then incubated at 25°C for 2 hours on a plate shaker shaking at 500 rpm.

Following incubation, the plate was washed with 1X wash buffer 3 times before 200 µl of the p-nitrophenyl phosphate (pNpp) substrate was added to the wells, followed by 1.5 hours of incubation at 25°C with shaking at 500 rpm. The enzymatic reaction was stopped by adding 50 µl of the Stop Solution, and the plate was placed in the BioTek Synergy Neo2 microplate reader (Agilent, Santa Clara, California, United States) immediately to read the absorbance at 405 nm. The average absorbance for each standard and sample was measured by subtracting the average absorbance of the blank. The average net OD for each standard and sample was calculated by subtracting the average non-specific binding absorbance measurement from the average absorbance measurement. The concentration (pmol/mL) of cAMP in tissue lysates was quantified by interpolation of net OD values in the standard curve (GraphPad Software, version 9 for Macintosh, San Diego, California, United States) and normalized by dividing by the total protein concentration (mg/mL).

Western blotting

The expression of the rate-limiting enzyme for triglyceride hydrolysis, HSL and p-HSL (Ser563) was quantified using the Western blotting technique as a marker of adrenergic receptor activation. Before working with samples from the first cohort of mice, an optimized Western blotting protocol was established for target proteins by trying different protein amounts, process of protein transfer, and dilution factors of primary and secondary antibodies (Table 2.1). Rather than using a housekeeping protein (β-actin, β-tubulin), total protein (100 to 37 kD) in each lane was used to normalize the target protein's expression. The specificity of HSL and p-HSL (Ser563) antibodies and expression of HSL and p-HSL (Ser563) protein

Table 2.1 A summary of experimental runs when optimizing the Western blotting protocol to identify the target proteins, hormone-sensitive lipase (HSL) and phospho-HSL (p-HSL) (Ser563). Protein was isolated from interscapular brown adipose tissue (iBAT) and the concentration was quantified (µg/mL) using a BCA assay. Different factors, such as protein amount (µg), antibody (primary and secondary) concentration, protein transfer technique, and chemiluminescence substrate were adjusted to find the optimal protocol.

Number of experiment	Resolving and stacking gels preparation	Protein amount	Protein transfer technique	Blocking buffer	Primary antibody concentration	Secondary antibody concentration	Chemiluminescence substrate
Run 1	10% resolving gel (0.75M Tris-HCl, 0.2% SDS, 9.84% bis-acrylamide, 0.06% APS, TEMED); 4% stacking gel (0.25M Tris-HCl, 0.2% SDS, 3.83% bis-acrylamide, 0.1% APS, TEMED)	25 µg (HSL and p-HSL)	Semi-dry transfer at 25 V for 45 minutes	5% BSA in PBS (0.1% tween 20)	1:1000 (HSL) 1:5000 (p-HSL)	1:3000 (HSL) 1:5000 (p-HSL)	Pierce™ chemiluminescence substrate*
Run 2	10% resolving and 4% stacking gels were prepared using the Tris-Glycine eXtended stain-free™ fastcast™ kit, 0.01% SDS, 0.05% APS, TEMED	15 µg (HSL) 25 µg (p-HSL)	Semi-dry transfer at 25 V for 45 minutes	5% BSA in PBS (0.1% tween 20)	1:3000 (HSL) 1:3000 (p-HSL)	1:5000 (HSL) 1:5000 (p-HSL)	Clarity Max™ enhanced chemiluminescence substrate
Run 3	As per Run 2	15 µg (HSL) 25 µg (p-HSL)	Wet transfer at 30 mA for 960 minutes	5% BSA in TBS (0.1% tween 20)	1:5000 (HSL) 1:1000 (p-HSL)	1:5000 (HSL) 1:5000 (p-HSL)	Clarity Max™ enhanced chemiluminescence substrate
Run 4	As per Run 2	10 µg (HSL) 25 µg (p-HSL)	Wet transfer at 30 mA for 960 minutes	5% BSA in TBS (0.1% tween 20)	1:10000 (HSL) 1:1000 (p-HSL)	1:5000 (HSL) 1:5000 (p-HSL)	Clarity Max™ enhanced chemiluminescence substrate

*Pierce™ chemiluminescence substrate (catalog no. 32109, ThermoFisher Scientific, Waltham, Massachusetts, United States)

in iBAT was assessed using the lung tissue as a negative control (Figure 2.5). Working with several tissues to assess the expression level of HSL by immunoblotting, lung tissue was identified as one of the tissues expressing a low amount of HSL protein (Kraemer et al. 1993). Based on the experimental evidence and tissue-specific HSL expression data in the National Center for Biotechnology Information, lung tissue was used as a negative control to confirm the HSL antibody specificity in iBAT samples. A standard curve (Figure 2.6) was also made for HSL and p-HSL (Ser563) using a series of protein amounts from a sample (n=1) giving maximum p-HSL (Ser563) protein band intensity and following the protocol described below.

Based on findings from protocol optimization and standard curve for HSL and p-HSL (Ser563), 10 µg of protein for HSL and 25 µg of protein for p-HSL were selected to run protein samples from both cohorts. The protein samples were prepared with MilliQ water and loading dye (0.25M Tris-HCl (pH 6.8), 20% (v/v) glycerol, 4.08% (w/v) sodium dodecyl sulfate (SDS), 0.1% (w/v) bromophenol blue). Two individual acrylamide gels (10% resolving gel and 4% stacking gel) were made for HSL and p-HSL (Ser563) using Tris-Glycine eXtended stain-free™ fastcast™ kit (catalog no. 1610182, Bio-Rad Laboratories, Hercules, California, United States), 0.05% (w/v) ammonium persulfate (APS), 0.01% (w/v) SDS, and 0.05% (v/v) tetramethylethylenediamine (TEMED). Protein samples and a protein ladder (catalog no. 1610373, Bio-Rad Laboratories, Hercules, California, United States) were loaded in gels and ran at 120V for an hour and 15 minutes. After the gel electrophoresis, the dye in the gel was activated for 45 seconds under the ChemiDoc imaging system (Bio-Rad Laboratories, Hercules, California, United States) to visualize proteins in gels. The Bio-Rad stain-free gel system includes a proprietary trihalo compound that binds to tryptophan

residues to enhance protein fluorescence after a brief ultraviolet activation provided by the imaging system.

The wet transfer process was followed to transfer proteins from the gel to 0.45 μm polyvinylidene fluoride (PVDF) membrane (catalog no. IPVH00010, MilliporeSigma, Burlington, Massachusetts, United States). The transfer sandwich in cassette was placed in the tank with transfer buffer (Tris-glycine (24.7 mM Tris, 191.8 mM glycine, pH 8.8), 20% (v/v) methanol, 0.025% (w/v) SDS, MilliQ water) for 16 hours at 30 mA. After the protein transfer, the PVDF membrane was visualized under the imaging system to get the total protein in each lane.

The membrane was blocked in 5% BSA (catalog no. a7906, Sigma Aldrich, St. Louis, Missouri, United States) in Tris-buffered saline (TBS) (4.8 mM Tris, 15.2 mM Tris-HCl, 150 mM NaCl, pH 7.6) (0.1% Tween 20) for 2 hours and incubated with blocking buffer diluted rabbit primary antibodies, 1:10000 diluted HSL (catalog no. 4107, Cell Signaling Technology, Danvers, Massachusetts, United States) and 1:1000 diluted p-HSL (Ser563) (catalog no. 4139, Cell Signaling Technology, Danvers, Massachusetts, United States), overnight at 4°C. The membrane was washed 3 times using TBS (0.1% Tween 20) and incubated with 1:5000 diluted goat anti-rabbit horseradish peroxidase-linked secondary antibodies (catalog no. 7074, Cell Signaling Technology, Danvers, Massachusetts, United States) for an hour. The membrane was washed again with TBS (0.1% Tween 20) 3 times and set under the imaging system to detect the target protein using the Clarity Max enhanced chemiluminescence substrate (catalog no. 1705062, Bio-Rad Laboratories, Hercules, California, United States). The exposure time was less than a minute to detect both targeted proteins. The ImageJ software was used to calculate the protein band density. Multiple gels

for one target protein were calibrated by dividing the protein band density values by the geomean of inter-gel calibrators (the first sample from each group). For samples where the p-HSL (Ser563) band is invisible, half of the minimum normalized protein band density value across gels was used as protein band density. HSL and p-HSL were individually normalized to total protein (100 to 37 kD). The normalized HSL and p-HSL (Ser563) values were further divided by the geomean of the saline group to calculate the relative expression of HSL and p-HSL. The bar graph (Figure 2.9B,C; 2.10B,C) was made by plotting the geometric mean value with 95% confidence interval.

Statistical Analysis

All data are presented as mean ± SEM and were analyzed by GraphPad Prism (GraphPad Software, version 9 for Macintosh, San Diego, California, United States). Each group consisted of n = 5-7, and 0.05 was set as the p-value to detect significant differences (p<0.05) in cAMP and relative p-HSL (Ser563) expression in iBAT among groups. The unpaired two-tailed t-test was used to compare between groups, and one-way analysis of variance (ANOVA) was used with multiple comparisons using Dunnett's test to detect differences in data obtained from Western blotting and cAMP assay between the groups.

2.3 RESULTS

Animals and iBAT Morphology

The overall body mass of mice before dissection did not differ significantly between groups (Figure 2.4A,C), which confirms the healthy growth of mice during the acclimation period. The mass of iBAT collected after dissection was not significantly different between groups (Figure 2.4B,D).

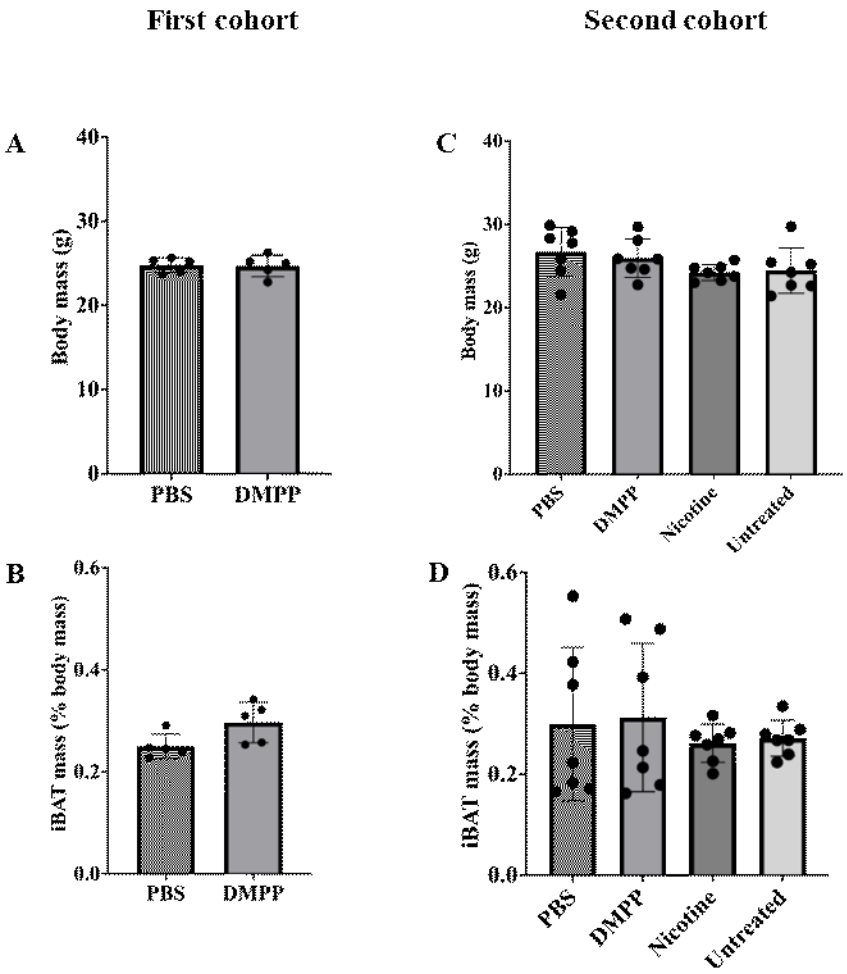

Figure 2.4 Whole body and interscapular brown adipose tissue (iBAT) mass (g). The overall body mass (g) of first cohort mice (**A**) and the mass of iBAT (% body mass) (**B**) were measured using a laboratory scale, and data were compared between groups (n=5) using an unpaired, two-tailed, student's t-test. No significant difference was identified between groups (p>0.05). The body mass (g) of the second cohort mice (**C**) and mass of iBAT (% body mass) (**D**) were measured using a laboratory scale, and analyzed using a one-way analysis of variance (ANOVA) followed by multiple comparisons tests using Dunnett's test to compare data between phosphate-buffered saline (PBS) control group and experimental groups (n=7). No significant difference between groups was identified.

Antibody Specificity and Standard Curves of HSL and p-HSL (Ser563)

The expression of HSL and p-HSL (Ser563) protein was found in iBAT samples, but not in the lung tissue sample (Figure 2.5). A linear graph was identified for HSL between 7.5 µg and 1.87 µg of protein (Figure 2.6A), and the linear graph for p-HSL (Ser563) was found between 30 µg and 7.5 µg of protein (Figure 2.6B).

cAMP assay Analysis

Treatment of the stellate ganglia with DMPP (100 µM), a nAChR agonist, did not alter the cAMP production in iBAT compared to the PBS-treated control group (p=0.3519) (Figure 2.7A,B).

Changing the approach of delivering DMPP to stellate ganglia and treating the stellate ganglia with nicotine (100 µM), another nAChR agonist, did not result in elevated cAMP production in iBAT compared to the PBS-treated control group (PBS vs DMPP: p=0.3064; PBS vs nicotine: p=0.6990) (Figure 2.8A,B). The untreated group, expected to produce a low amount of cAMP in iBAT compared to the PBS-treated control group, was not found to be significantly different than the PBS-treated control group (p=0.0553) (Figure 2.8B).

Relative Expression of HSL and p-HSL (Ser563) in iBAT

The expression of HSL (83 kD) protein was detected in all iBAT samples collected after delivering PBS and DMPP to the stellate ganglia (Figure 2.9A,C); however, p-HSL (Ser563) (83 kD) protein was detected in 4 out of 5 PBS and DMPP-treated samples (Figure 2.9A). Treatment of the stellate ganglia with DMPP (100 µM) did not increase the relative expression of p-HSL (Ser563) compared to the PBS-treated control group (p=0.2342) (Figure 2.9B).

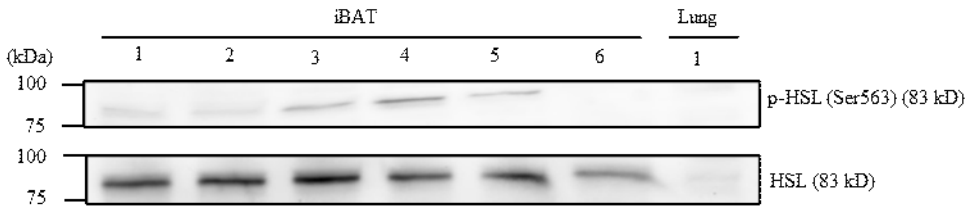

Figure 2.5 Expression of hormone-sensitive lipase (HSL) (83 kD) and phospho-HSL (p-HSL) (Ser563) (83 kD) protein in interscapular brown adipose tissue (iBAT) (positive control) (n=6) and lung tissue (negative control) (n=1) (the entire blot with protein ladder images are in Figure A2 of appendix). 15 µg of protein for HSL and 25 µg of protein for p-HSL were loaded on to gels, proteins were transferred from the gel to a polyvinylidene fluoride (PVDF) membrane, the membrane was incubated with primary antibodies (1:5000 HSL, 1:5000 p-HSL (Ser563)), later secondary antibodies (1:5000 goat anti-rabbit) and visualized by chemiluminescence substrate.

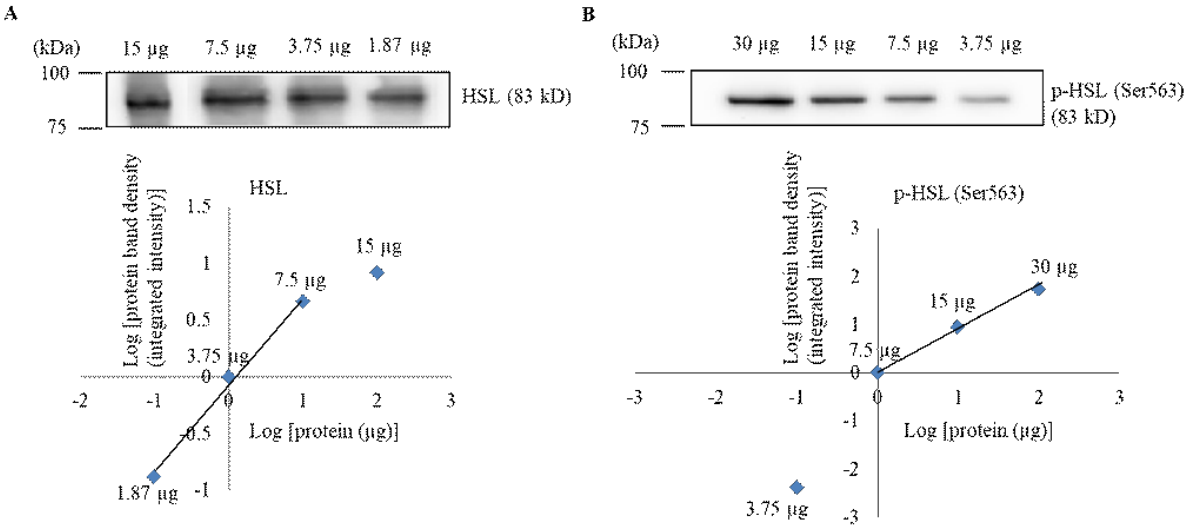

Figure 2.6 A standard curve for the detection of hormone-sensitive lipase (HSL) and phospho-HSL (p-HSL) (Ser563) protein using Western blotting. A series of protein amounts (1.87-30 µg) from an interscapular brown adipose tissue (iBAT) sample (n=1) giving maximum p-HSL (Ser563) protein band intensity was run following the Western blotting protocol. **A.** Expression of HSL (83 kD) in protein samples ranging from 15 µg to 1.87 µg of protein. The membrane was incubated with 1:10000 anti-HSL antibody and 1:5000 secondary antibody. HSL band of all protein amounts was normalized to HSL band of 3.75 µg protein, and a linear graph was found between 7.5 µg and 1.87 µg of protein. **B.** Expression of p-HSL (Ser563) (83 kD) in protein samples ranging from 30 µg to 3.75 µg of protein. The membrane was incubated with 1:1000 anti-p-HSL (Ser563) antibody and 1:5000 secondary antibody. p-HSL band of all protein amounts was normalized to p-HSL band of 7.5 µg protein, and a linear graph was found between 30 µg and 7.5 µg of protein. Images were analyzed by ImageJ software.

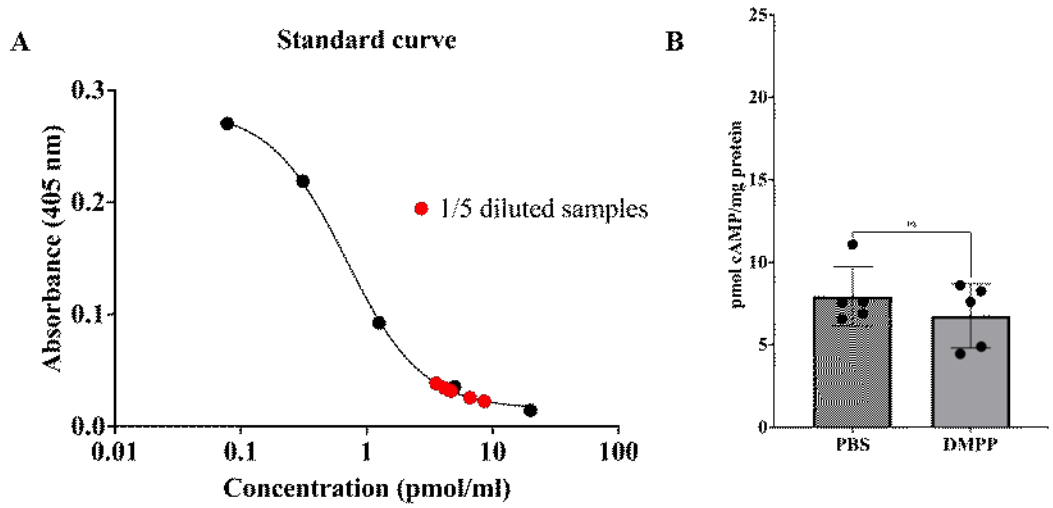

Figure 2.7 The concentration of cAMP in interscapular brown adipose tissue (iBAT) samples (first cohort) collected after treating the stellate ganglia with phosphate-buffered saline (PBS) and dimethylphenylpiperazinium (DMPP) (100µM). **A.** A standard curve for cAMP concentration ranging from 20 to 0.078 pmol/mL generated by following the competitive ELISA technique. Tissue lysates were diluted (1:5) in 0.1M HCl and loaded onto the anti-rabbit antibody coated 96-well plate, alkaline phosphatase conjugated-antigen and rabbit antibody were aliquoted to wells, respectively, pNpp substrate was added to wells after washing the plate, and the absorbance reading was taken at 405 nm after adding the stop solution. **B.** Quantification of cAMP concentration (pmol/mL) was normalized to protein concentration (mg/mL). An unpaired, two-tailed *t*-test was used to compare cAMP quantities between groups (n=5), and no significant difference (ns) between groups was identified.

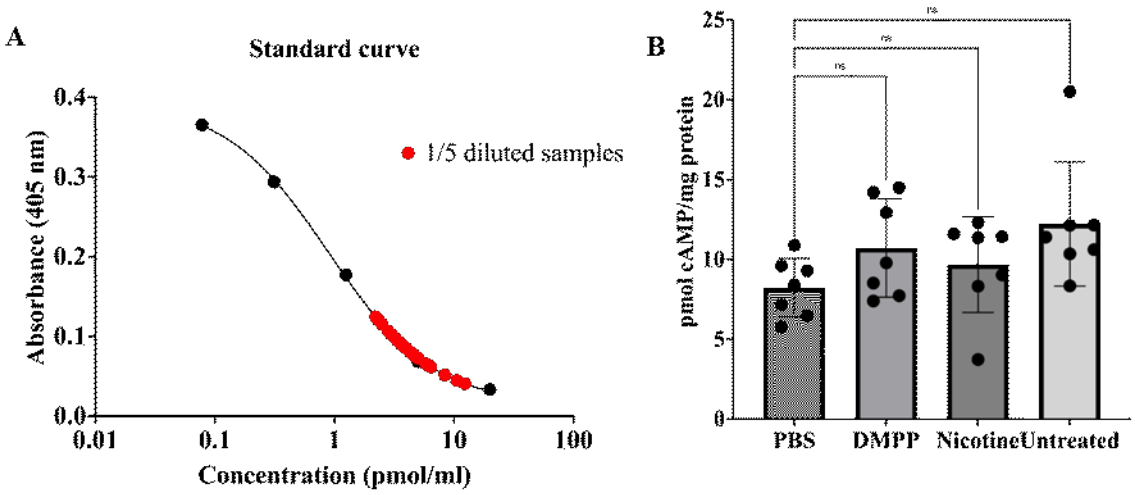

Figure 2.8 The concentration of cAMP in interscapular brown adipose tissue (iBAT) samples (second cohort) collected after treating the stellate ganglia with phosphate-buffered saline (PBS), dimethylphenylpiperazinium (DMPP) (100µM), nicotine (100µM), and without treatment. **A.** A standard curve for cAMP concentration ranging from 20 to 0.078 pmol/mL generated by following the competitive ELISA technique. Tissue lysates were diluted (1:5) in 0.1M HCl and loaded onto the anti-rabbit antibody coated 96-well plate, alkaline phosphatase conjugated-antigen and rabbit antibody were aliquoted to wells, respectively, pNpp substrate was added to wells after washing the plate, and the absorbance reading was taken at 405 nm after adding the stop solution. **B.** Quantification of cAMP concentration (pmol/mL) was normalized to protein concentration (mg/mL). A one-way analysis of variance (ANOVA) was used followed by a multiple comparisons test using Dunnett's test to compare cAMP quantities between PBS control group and experimental groups (n=7). No significant difference (ns) between groups was identified.

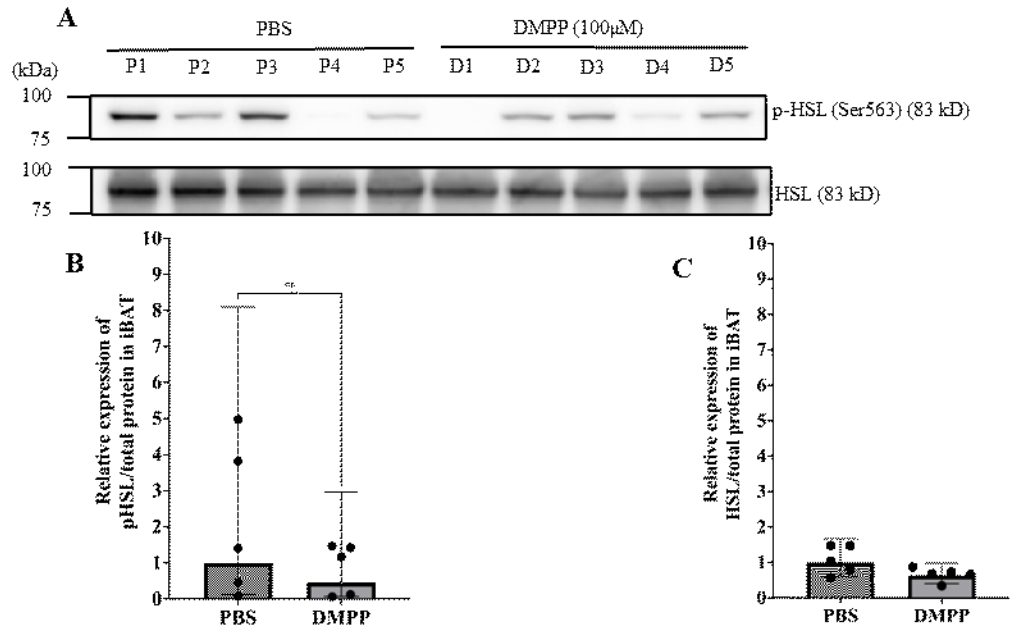

Figure 2.9 Expression of hormone-sensitive lipase (HSL) (83 kD) and phospho-HSL (p-HSL) (Ser563) (83 kD) protein in interscapular brown adipose tissue (iBAT) samples (first cohort) collected after treating the stellate ganglia with phosphate-buffered saline (PBS) and dimethylphenylpiperazinium (DMPP) (100μM). **A.** Representative Western blot images of HSL and p-HSL (Ser563) expression (the entire blot with protein ladder images are in Figure A3 of appendix). 10 μg of protein for HSL and 25 μg of protein for p-HSL were loaded on to gels, proteins were transferred from the gel to a polyvinylidene fluoride (PVDF) membrane, the membrane was incubated with primary antibodies (1:10000 HSL, 1:1000 p-HSL (Ser563)), later secondary antibodies (1:5000 goat anti-rabbit) and visualized by chemiluminescence substrate. **B.** Densitometric analysis of p-HSL (Ser563) was normalized to total protein (100-37 kD), **C.** Densitometric analysis of HSL (83 kD) was normalized to total protein (100-37 kD). The geometric mean value with 95% confidence interval was plotted to make the bar graph. Half of the minimum normalized protein band density value was used for samples (PBS: P4; DMPP: D1) expressing no visible p-HSL protein band. An unpaired, two-tailed *t*-test was used to compare relative protein quantities between groups (n=5), with no significant difference (ns) between groups identified.

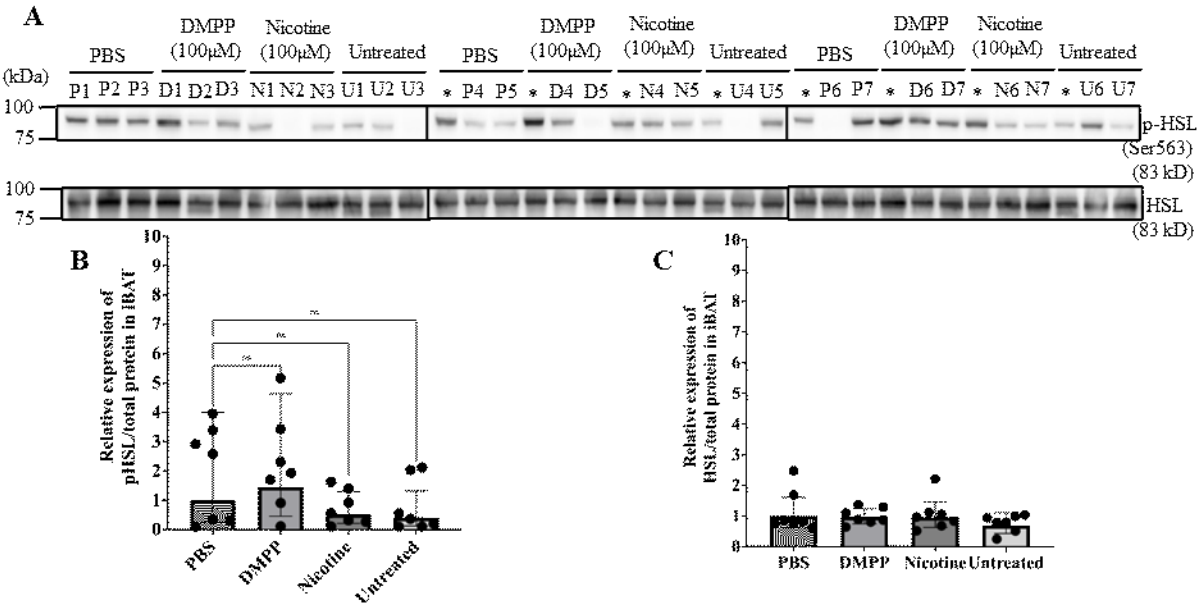

Figure 2.10 Expression of hormone-sensitive lipase (HSL) (83 kD) and phospho-HSL (p-HSL) (Ser563) (83 kD) protein in interscapular brown adipose tissue (iBAT) samples (second cohort) collected after treating the stellate ganglia with phosphate-buffered saline (PBS), dimethylphenylpiperazinium (DMPP) (100μM), nicotine (100μM), and without treatment. **A.** Representative Western blot images of HSL and p-HSL (Ser563) expression (the entire blot with protein ladder images are in Figure A4, A5, and A6 of appendix). Asterisks (*) denotes the inter-gel calibrators (the first sample from each group). 10 μg of protein for HSL and 25 μg of protein for p-HSL were loaded on to gels, proteins were transferred from the gel to a polyvinylidene fluoride (PVDF) membrane, the membrane was incubated with primary antibodies (1:10000 HSL, 1:1000 p-HSL (Ser563)), later secondary antibodies (1:5000 goat anti-rabbit) and visualized by chemiluminescence substrate. **B.** Densitometric analysis of p-HSL (Ser563) was normalized to total protein (100-37 kD), **C.** Densitometric analysis of HSL (83 kD) was normalized to total protein (100-37 kD). The geometric mean value with 95% confidence interval was plotted to make the bar graph. Half of the minimum normalized protein band density value across gels was used for samples (PBS: P6; DMPP: D5; nicotine: N2; untreated: U3, U4) expressing no visible p-HSL protein band. A one-way analysis of variance (ANOVA) was used followed by a multiple comparisons test using Dunnett's test to compare relative protein quantities between PBS control group and experimental groups (n=7), and no significant difference (ns) between groups was identified.

A different approach applied to the second cohort mice injecting nAChR agonists into the stellate ganglia did not alter the relative expression of p-HSL (Ser563) in iBAT compared to the PBS-treated control group (PBS vs DMPP: p=0.9544; PBS vs nicotine: p=0.2225) (Figure 2.10B). The expression of HSL (83 kD) protein was detected in all iBAT samples (Figure 2.10A,C), but p-HSL (Ser563) (83 kD) protein was detected in 6 out of 7 PBS, DMPP, and nicotine-treated and 5 out of 7 untreated samples (Figure 2.10A). Using nicotine (100 μM) as a second nAChR agonist did not increase the relative expression of p-HSL (Ser563) in iBAT compared to the PBS-treated control group (p=0.2225) (Figure 2.10B). Although the untreated group was expected to provide a baseline expression of p-HSL (Ser563) in iBAT collected without touching the stellate ganglia, this group was not found to be significantly different than the PBS-treated control group (p=0.2446) (Figure 2.10B).

2.4 DISCUSSION

It is well-established that PACAP has a role in augmenting the cholinergic stimulation of catecholamine release at the sympatho-adrenomedullary axis (Eiden et al. 2018; Stroth et al. 2013); however, the action of PACAP in catecholamine release at peripheral SNS has not been measured directly. We developed an *ex vivo* model and focused on the stellate ganglia to study PACAP's role in catecholamine release and stimulating downstream adrenergic signaling in iBAT. The assessment of the model using two nAChR agonists demonstrated that our model is unsuccessful in stimulating the expression of molecular markers (cAMP, p-HSL (Ser563)) of the adrenergic signaling (Figure 2.7-2.10). The identification of PACAP expression in preganglionic nerves and the expression of the PAC1 receptors in postganglionic neurons of the superior cervical ganglia suggests functionality of PACAP signaling in peripheral ganglia (Beaudet et al. 1998; Braas and May

1999), but direct evidence of contribution to catecholamine release has not been identified. One member of our lab was able to show the presence of PACAP in synaptic vesicles adjacent to postganglionic cell bodies of the stellate ganglia using the immunohistochemistry technique (data not shown, unpublished). The expression of PACAP receptors (PAC1, VPAC1) in postganglionic neurons of the stellate ganglia was confirmed by a member of our lab (Pandher et al. 2023); however, the function of these receptors at ganglia is not known, which intrigued us to address the functional significance of these receptors in catecholamine release using an *ex vivo* model.

Developing an *ex vivo* model was the first challenging step for this thesis, considering the experimental approach to deliver nAChR agonists to the ganglia, which could contribute to neuronal firing and manipulate the experimental data. The inability of nAChR agonists to increase cAMP and p-HSL (Ser563) production (Figure 2.7-2.10) in iBAT provides insight into the challenges of studying a sympathetic ganglion using an *ex vivo* model. The small size and complex structure of the ganglia containing a cluster of nerve cell bodies made it challenging to confirm the delivery of nAChR agonists to the ganglia. Since the peripheral ganglia, one of the stress-responsive pathways, was the experimental focus of this thesis, minimizing the environmental stress on the model was crucial to avoid activation of the stress pathway by environmental stressors. Considering all these factors, optimizing the mice dissecting protocol and approach to deliver nAChR agonists to ganglia were critical to validate further experimental data. Optimizing molecular techniques was also essential for robust quantification of molecular markers in iBAT.

HSL is a hallmark of norepinephrine-stimulated adrenergic signaling in BAT (Cannon and Nedergaard 2004; Duncan et al. 2007). The activation properties of HSL are

present in its phosphorylated form, and it has been found that HSL can be phosphorylated by PKA at multiple positions (Ser563, Ser659, Ser660) (Anthonsen et al. 1998). While we had aimed to assess the induction of multiple forms of p-HSL as a molecular readout of our protocol, an 83 kDa band was not detected in iBAT protein extracts using the p-HSL (Ser660)-specific antibody (Figure A1 in appendix) in our protocol optimization step. However, the p-HSL (Ser563)-specific antibody revealed the positive immunoreactivity with a band at 83 kDa (Figure 2.9A, 2.10A). While I was not able to continue with both antibodies, p-HSL (Ser563) was decided to be a robust molecular marker of HSL activity, as most of the studies related to BAT activation and function in the literature have focused on the Ser563 position (Arisawa et al. 2024; Cero et al. 2020), considering Ser563 has been found to be the primary phosphorylation site of HSL (Belfrage et al. 1997; Garton et al. 1988). A positive immunoreactivity of p-HSL (Ser563) antibody was identified using *in vitro*, *in vivo*, and *ex vivo* models with different experimental conditions (Abe, Sato, and Murotomi 2023; Arisawa et al. 2024; Cero et al. 2020; Zhu et al. 2019), validating the specificity of the antibody. As such, the p-HSL (Ser563)-specific antibody was used in subsequent experiments to quantify the relative expression of p-HSL in BAT collected after stimulating the stellate ganglia with nAChR agonists.

Based on the literature review, the ratio of p-HSL to HSL was found to be a well-established parameter to assess the sympathetic activation of BAT and thermogenesis via lipolysis (Abe, Sato, and Murotomi 2023; Arisawa et al. 2024; Cero et al. 2020; Zhu et al. 2019). However, standard curves for HSL and p-HSL accuracy and limits of detection were not found in papers. As such, we generated standard curves for HSL and p-HSL (Ser563) (Figure 2.6) and plotted the pooled sample from each group to identify the ideal protein

amount and antibody concentration to support semi-quantitative analysis of Western blotting for both proteins (HSL and p-HSL). The linear curve of the p-HSL (Ser563) antibody at the conditions tested demonstrated it could be used for reliable quantification; however, the HSL antibody was found to be inconsistent in terms of sensitivity and provided a high background signal that raised concerns about using HSL expression as a denominator to calculate the relative expression of p-HSL. As a result, we normalized the p-HSL protein to total protein rather than HSL to find the relative expression of p-HSL in iBAT.

Despite DMPP is a well-established nAChR agonist, the production of cAMP and relative expression of p-HSL (Ser563) were not increased in iBAT collected after treating the stellate ganglia with 100 μM DMPP (Figure 2.7B, 2.9B). It is possible that the ability of DMPP to stimulate the nAChR may have been masked by the extracellular matrix and vascular tissues that obstacle the delivery of DMPP to sympathetic nerve cells. To assess this, a new approach for delivery of DMPP was applied to the second cohort where DMPP solution was injected into the stellate ganglia; however, injecting DMPP into the stellate ganglia did not elicit an elevated cAMP production and relative expression of p-HSL (Ser563) in iBAT (Figure 2.8B, 2.10B). Previous work has reported that incubation of intact superior cervical ganglia in a medium containing 100 μM DMPP increased the DOPA production fivefold (Horwitz and Perlman 1984).

Another nAChR agonist, nicotine, tried with the second cohort did not augment cAMP production and relative expression of p-HSL (Ser563) in iBAT (Figure 2.8B, 2.10B). Previous reports have shown that incubation of the primary cultured (a splanchnic nerve-free *in vitro* system) bovine adrenal chromaffin cells in a medium containing 10 μM nicotine elevated endogenous catecholamine release (Mizobe and Livett 1983), which was consistent

with findings from a similar experiment worked with ACh to evoke the catecholamine release (Livett et al. 1979). Our *ex vivo* model required the selection of a higher nicotine dose (100 μM) than used in the *in vitro* system, but the dose was not higher than the threshold ($>10^{-4}$ M) that causes desensitization of the nAChR (Thesleff and Katz 1957), so it is unlikely that 100 μM nicotine dose could inhibit nicotine's ability to activate the nAChR.

In trying to speculate why I was not able to achieve stimulation of cAMP or p-HSL with DMPP or nicotine, it is possible that the 3-minute nAChR agonist incubation period may not be adequate to observe the ganglia stimulation effect on adrenergic signaling in iBAT. Previous time course experiments reported that the first 15 minutes of DMPP incubation elicited the maximum nAChR response to produce DOPA, a precursor compound of catecholamine synthesis, in superior cervical ganglia (Horwitz and Perlman 1984). Another relevant research showed that 90 to 100% of maximum catecholamine release from adrenal chromaffin cells occurred within 5 minutes of nicotine incubation (Mizobe and Livett 1983). Unlike culturing the chromaffin cells in the *in vitro* system where a treatment reagent directly accesses the cell environment, we used an *ex vivo* model and focused on a peripheral ganglia where the sympathetic nerve cells, our experimental focus, are covered by dense connective tissue, vascular tissue, and extracellular matrix (Gray 2008), which might demand a higher dose and long incubation time for the nAChR agonist solutions to reach the sympathetic nerve cells. We focused on analyzing the preganglionic neurons secreted catecholamine effect on adrenergic signaling in iBAT innervated by the long postganglionic neuron of the peripheral ganglia, which might require a long incubation time than 3 minutes to observe the ganglia stimulation effect on downstream adrenergic signaling cascade in iBAT.

It was surprising that the PBS-treated group (vehicle control) and the DMPP-treated group expressed near similar levels of p-HSL (Ser563) and cAMP in iBAT (Figure 2.7B, 2.9B), which indicates touching the ganglia by dissection tools might cause the neuronal firing. In order to analyze the cause of unexpected increase in p-HSL (Ser563) and cAMP production in the PBS-treated group, we added an untreated group to the second cohort where the iBAT was collected without exposing the ganglia. Although there was no significant difference between the PBS and untreated group based on the relative expression of p-HSL (Ser563) in iBAT (Figure 2.10B), the *p*-value was very close to significance (p=0.0553) according to the cAMP level (Figure 2.8B) between groups. It is possible that dissection tools may influence the activation of nAChR, and delivering the nAChR agonists may cause desensitization of the receptor, which results in the inactivation of ion channels and reduction of the nicotinic receptor response (Kandel et al. 2021). Based on these data, it is likely that our experimental approach is not ideal to observe the actual stimulation of nAChR by nAChR agonists in the stellate ganglia.

From the statistical perspective, it is possible that due to using a small sample size (n = 5-7) for each group, there may not have been enough statistical power to detect a difference between groups. The data (Figure 2.7B, 2.8B, 2.9B, 2.10B) from our experiments represent variability with a high standard deviation in each group, which means more overlap between two distributions and less power to detect a difference between groups. Ideally, a power calculation would be conducted prior to starting the experiment to estimate the sample size necessary to detect a difference between groups (Howell 2013). The power analysis of a study depends on multiple factors, and one of the essential factors is a predefined effect size (Howell 2013). We developed an *ex vivo* model and used a novel approach to stimulate the

ganglia by nAChR agonists, hence the effect size was not available in the literature. Since the relevant effect size and actual variability within the data were not known, a power calculation was not completed. Considering a novel experimental approach without a known probable effect size and using animals as a model that raises ethical concerns, we decided to use a small sample size (n = 5) for the first cohort to validate the experimental model and approach first. To provide more statistical power to minimize the overlap of means from different distributions and detect a difference between groups, we decided to increase the sample size (n = 10) for the second cohort. However, we had to exempt some mice from the experimental design due to their aggressive behavior and stress, which reduced the sample size to n=7 for each group.

In order to reduce the variability, a few factors were considered in the experimental design, including using an inbred mouse strain (backcrossed C57B16 mouse line), the established anatomical landmark to detect the stellate ganglia precisely, and molecular techniques known to be sensitive, specific, and efficient to detect molecules, such as cAMP and proteins (competitive ELISA and Western blotting, respectively).

2.5 CONCLUSION

Experimental evidence in the literature demonstrates that PACAP has a role in regulating catecholamine secretion at the sympatho-adrenomedullary axis; however, PACAP's role in peripheral sympathetic ganglia is not well-characterized. While we aimed to develop an *ex vivo* model to study the effect of PACAP on catecholamine activity in BAT, model testing using two nAChR agonists (DMPP, nicotine) was unsuccessful. Both potential nAChR agonists failed to increase the expression of molecular markers (cAMP, p-HSL (Ser563)) of the adrenergic signaling, even though DMPP and nicotine are well-known for

nicotinic receptor stimulatory action in SNS. According to our experimental data, further modification to the protocol or an alternate approach will need to be developed to analyze PACAP receptor function in the peripheral sympathetic ganglia. Alternative approaches could include, incubating the intact stellate ganglia or primary cultured postganglionic neurons in a PACAP-containing medium. Further attempts to develop such a model will support experiments designed to enhance the understanding of PACAP's role in regulating catecholamine synthesis and release in peripheral ganglia.

Chapter Three: Concluding Remarks and Future Prospects on Investigating PACAP's Functional Role in Peripheral Ganglia

3.1 SUMMARY

The work presented in this thesis aimed to enhance our understanding of the role of PACAP in peripheral SNS, specifically, the functional role of activated PACAP receptors located in peripheral ganglia in regulating catecholamine secretion and peripheral effector organ activation. In support of this, Chapter Two presents data that demonstrate an approach to develop and assess an *ex vivo* model to study the function of PACAP receptors in the stellate ganglia. The objectives for generation of this model were the following:

1. Develop an *ex vivo* model and validate the model and experimental approach by using two nAChR agonists (DMPP, nicotine) before working with PACAP.
2. Assess two molecular markers (cAMP, p-HSL (Ser563)) of the adrenergic signaling in iBAT collected after administering the nAChR agonist to the stellate ganglia.
3. Optimize the protocol of two molecular techniques, competitive ELISA and Western blotting, and measure the expression of cAMP and p-HSL (Ser563) in iBAT following the above techniques, respectively.

Chapter Two addressed objectives 1 to 3 above, first developing a novel dissection protocol to stimulate the stellate ganglia by delivering nAChR agonists. I then measured the expression of cAMP and p-HSL (Ser563) in iBAT, expecting ganglia stimulation to increase these molecular markers levels. DMPP (100 μM) administered to the stellate ganglia by dropping or injecting into the ganglia did not elevate the level of cAMP and p-HSL (Ser563) in iBAT compared to vehicle administration (Figure 2.7-2.10). These negative findings directed us to try another nAChR agonist (nicotine, 100 μM) to stimulate the stellate ganglia. Injecting the nicotine solution into the stellate ganglia also did not augment the expression of cAMP and p-HSL (Ser563) in iBAT (Figure 2.8, 2.10) compared to vehicle treatment. These

results demonstrate that the novel experimental model and approach for stimulation were not successful in stimulating the stellate ganglia, and a different method will need to be tested to study PACAP's functional role in the peripheral ganglia of the SNS.

Chapter Three will discuss the future aims and experimental design to study PACAP's role in the stellate ganglia by using other approaches or modifications to the method (*in vivo* or *in vitro*). The necessity of PACAP to sustain the secretion of catecholamine under a stress condition has been well-characterized in adrenal chromaffin cells (Eiden et al. 2018; Stroth et al. 2013). Finding the expression of PACAP in preganglionic synaptic vesicles and PACAP receptors in postganglionic neurons supports the presence of PACAP signaling in the peripheral ganglia (Beaudet et al. 1998; Pandher et al. 2023). The cold-sensitive phenotype and low norepinephrine content found in the iBAT of PACAP null mice suggest the role of PACAP in thermogenesis in response to cold stress (Diané et al. 2014; Gray et al. 2002). Considering all experimental evidence, it is convincing that PACAP must have a role in regulating catecholamine release under stress. Unfortunately, assessment of the model described in Chapter Two using a novel dissection approach to deliver two nAChR agonists to the ganglia did not result in an increased level of downstream markers of adrenergic signaling in iBAT and thus is not ideal for studying PACAP's function in the peripheral ganglia. These results have motivated me to consider different methods to explore the functional role of PACAP and its receptors in the peripheral SNS.

3.2 FUTURE EXPERIMENTS WITH PACAP

PACAP has been identified in both central and peripheral nervous systems involved in regulating the sympathetic response to systemic and psychogenic stress (Gray and Cline

2019; Mustafa 2013). It has been shown that PACAP is a principle neurotransmitter responsible for catecholamine release during stress (Eiden et al. 2018). Finding a low level of norepinephrine in iBAT of PACAP null mice introduced to cold stress also suggested a role for PACAP in catecholamine secretion (Gray et al. 2002). PACAP displays physiological functions through binding with three receptors: PAC1, VPAC1, and VPAC2. All three PACAP receptors belong to class B GPCRs, the Secretin family of GPCRs that have been found to relate to pathophysiology (Couvineau and Laburthe 2012), thus getting attention for further study as therapeutic targets for disease. In addition to PACAP, there are other ligands, such as VIP, that bind with class B GPCRs. The N-terminal domain and transmembrane domain seven of GPCRs recognize and bind with ligands, which trigger a conformational change of the receptor, resulting in up-regulation or down-regulation of the downstream signaling cascades (Duc, Kim, and Chung 2015).

As described in section 1.7 of Chapter 1, alternative splicing generates functional diversity in PACAP receptors by changing the amino acid sequence. Radio-ligand binding studies revealed ligand specificity of the three PACAP receptors. VPAC1 and VPAC2 have higher affinity for VIP than PACAP, and PAC1 has 100-fold more affinity for PACAP than VIP (Harmar et al. 2012) (Table 1.1). Besides the endogenous ligands, there are some synthetic peptides (Table 1.1) that have an affinity for the PACAP specific receptor. The differences in ligand affinity impact the receptor's mechanism of action and downstream signaling.

The presence of the PAC1 receptor in the adrenal chromaffin cells involved in catecholamine secretion is well-studied (Eiden et al. 2018). The PAC1 receptor was also found in the postganglionic neuron of the superior cervical ganglia (Braas and May 1999).

Two of three PACAP receptors (PAC1, VPAC1) have been identified in the stellate ganglia with one N-terminal splice variant and two third intracellular loop splice variants of PAC1 receptor (Pandher et al. 2023); however, the functional role of these receptors and selectivity to ligands are not characterized. Given the negative results described in Chapter Two, using these known agonist and antagonist molecules (Maxadilan, M65, and PACAP 6-38) to assess PACAP receptor activity in the ganglia will require a modified or novel approach.

Suggested Modifications to Current Model

Before the model is abandoned, the sample size will be increased (n = 10) for future experiments to provide enough statistical power to detect a difference between groups. In order to find reliable and reproducible data, designing the experiment and methodology is crucial before conducting the experiments. Calculating the sample size is an essential component of experimental design, as a small sample size may produce inconclusive results, and a large sample size may produce statistically significant but biologically irrelevant results. In addition, an overly large sample size raises ethical concerns about the waste of resources, including animal lives (Charan and Kantharia 2013; du Sert et al. 2020). Therefore, the sample size should be calculated using a power calculation. However, as previously described in the discussion of Chapter Two, power calculations are challenging to conduct for studies that use a novel experimental approach to observe physiological changes in animals.

Based on the updated Animal Research: Reporting *In Vivo* Experiments (ARRIVE) guidelines (Percie du Sert et al. 2020; du Sert et al. 2020), sample size counting relies on the purpose of the study. In this thesis, our objective was to determine the function of PACAP receptor activation in the stellate ganglia by assessing downstream markers of adrenergic

signaling. A power analysis depends on predefined, biologically relevant effect size, estimated variability, significance level, and sample size (Howell 2013; du Sert et al. 2020). The possible effect size and estimated variability within the measurements were not known to us, considering that we were using a novel approach to stimulate the ganglia. As a result, we could not do the power calculation to estimate the sample size. Another ANOVA-based formula used to determine the sample size is the calculation of the E value. The E value is determined by subtracting the total number of groups from the total number of animals used in the experiment (Charan and Kantharia 2013). The E value of less than 10 indicates that adding more samples will increase the chance of finding a difference between groups, which was the case for the first cohort mice (E=8) used in this thesis. The E value of more than 20 indicates that it is unlikely to find a difference between groups by adding more samples (Charan and Kantharia 2013), which was the case for the second cohort mice (E=24). However, this formula is not as robust as a power calculation.

Suggested Future Model

The primary culture of postganglionic neurons can be a potential *in vitro* model for studying the role of activated PACAP receptors in the stellate ganglia in regulating catecholamine release. The primary culture of postganglionic sympathetic neurons is a well-established model to characterize receptors that regulate catecholamine release. The electrophysiological experiments demonstrated that the primary culture of mouse postganglionic sympathetic neurons dissociated from the ganglia is a robust model for the study of norepinephrine secretion (Trendelenburg et al. 1999). The cultured neurons develop short dendrites and axon branches that interconnect with soma bodies and form synaptic contacts. Soma and somato-dendritic regions have been found to hold receptors (nicotinic

and muscarinic AChRs, PACAP and VIP receptors, etc.) regulating catecholamine release, and the branching axons have been identified as the major site of catecholamine release (Boehm and Huck 1997). There are two methods to dissociate the postganglionic neurons from the ganglia: 1. mechanical agitation, 2. enzymatic action (trypsin, papain, collagenase, and dispase) followed by trituration (Boehm and Huck 1997).

Following the protocol for primary culture of postganglionic neurons described by May, Brandenburg, and Braas (1995), the stellate ganglia will be dissected from mice, and the postganglionic neurons will be dissociated by trituration. The cell suspension found after trituration will be plated onto a culture dish containing culture medium, nerve growth factor, and other components. The culture dish will be incubated at 37°C for 7 days in an atmosphere of 5% CO_2/95% air to grow the nerve cells. After 1.5 days, cytosine β-D-arabinofuranoside will be added to the culture dish for 24 hours to reduce non-neuronal cell growth. The culture medium will be replaced with the fresh medium after 3 days. On day 7, cells will be fixed and incubated with anti-TH antibodies to confirm the presence and growth of postganglionic neurons. An aliquot of PACAP receptor agonist and antagonist (Table 1.1) solution will be added to the culture dish to incubate cells with agonist and antagonist compounds at 37°C for a period of time. Afterwards, cells will be extracted in an acid solvent and will be centrifuged along with the culture medium to quantify the catecholamine amount in cells and released into the medium. The electrochemical catecholamine assays following reversed phase high-performance liquid chromatography (HPLC) will be used to assess catecholamine and metabolite levels in cells and medium (May, Brandenburg, and Braas 1995).

Primary cell culture is the best representative of *in vivo* biology, being recognized as

an ideal model for analyzing the effects of treatment on physiological changes. This model confirms the same genetic background of all cells, thus reducing the physiological variability. The monolayer cultures of dissociated postganglionic neurons confirm that receptors in postganglionic neurons activated by treatment compounds are the only source of catecholamine secretion. Our *ex vivo* model was challenging from this perspective, where the technical approach might influence receptor activation. The primary culture of dissociated neurons allows direct access of treatment compounds to the cell environment, which results in quick response of receptors to low concentrated treatment compounds (high potency) and stimulation of signaling cascade. Our *ex vivo* model, on the contrary, focused on the intact ganglia that demand a higher dose of treatment and long incubation time compared to the *in vitro* model to depolarize receptors. While the advantages of primary cell culture make it a promising *in vitro* model, some drawbacks also persist, including easy contamination of medium, limited lifespan of cells, and high costs of medium components. All these limitations of the *in vitro* model made us interested in developing an *ex vivo* model, which could be a potential model for pharmacological studies if the model was successful.

3.3 SIGNIFICANCE

Obesity is one of the world's contemporary health concerns, getting serious attention for its detrimental effect on quality of life and the economic burden of health care. The conventional idea of managing body weight by following a proper meal plan and physical exercise has been unsuccessful in restraining the growing rate of obesity in our population. A coordinated action of nutritional, hormonal, and neuronal signals is involved in regulating energy homeostasis. The connection of neuroendocrine to energy metabolism is an expanding area of research to identify potential therapeutic targets for treating obesity.

PACAP is a neuropeptide that functions via SNS, and one of its major functions is inducing thermogenesis in iBAT. Adaptive thermogenesis is an energy expenditure mechanism that contributes to maintaining energy homeostasis. This thesis aimed to characterize PACAP's role in regulating BAT function, thus this work will help in understanding the potentiality of PACAP as a therapeutic target to combat metabolic diseases.

The preliminary assessment of our model using nAChR agonists elucidates the challenge of working with an *ex vivo* model focusing on the sympathetic ganglia, which are very small structures that may fire with handling or become unable to be stimulated by following the dissection protocol. This thesis developed an *ex vivo* model, which could be a potential alternative to *in vitro* model associated with a few limitations. Our *ex vivo* model could create an exciting opportunity to further study PACAP receptor's specificity by using agonist and antagonist molecules and the connection of PACAP to the larger context of energy homeostasis if the model was successful. We established an optimized Western blotting and cAMP assay protocol and made standard curves for HSL and p-HSL (Ser563), which will be a significant addition to future studies investigating BAT activation and thermogenesis. Collected iBAT after ganglia stimulation will be a valuable resource for Gray lab to analyze the catecholamine content in iBAT in collaboration with the National Institute of Health, which will make a more robust conclusion of this thesis.

In summary, this thesis has contributed to understanding the challenge of studying the effect of sympathetic ganglia stimulation on peripheral organs *in vivo*, considering the long axons of postganglionic fibers that may slow down the action potential signals to release catecholamine and activate the target tissue. The results of this thesis will inform the Gray lab's next steps, such as their decision to use a different method (*in vivo* or *in vitro*) to

address the functional role of PACAP receptors in peripheral ganglia. Outcomes from future experiments demonstrating the function of PACAP and its receptors in peripheral ganglia will enhance the understanding of PACAP's role in SNS physiology.

REFERENCES

Abe, Tomoki, Tomoyuki Sato, and Kazutoshi Murotomi. 2023. "Sudachitin and Nobiletin Stimulate Lipolysis via Activation of the CAMP/PKA/HSL Pathway in 3T3-L1 Adipocytes." *Foods* 12(10):1–14. doi: 10.3390/foods12101947.

Althaher, Arwa R. 2022. "An Overview of Hormone-Sensitive Lipase (HSL)." *The Scientific World Journal*. doi: 10.1155/2022/1964684.

Anthonsen, Marit W., Lars Rönnstrand, Christer Wernstedt, Eva Degerman, and Cecilia Holm. 1998. "Identification of Novel Phosphorylation Sites in Hormone-Sensitive Lipase That Are Phosphorylated in Response to Isoproterenol and Govern Activation Properties in Vitro." *Journal of Biological Chemistry* 273(1):215–21. doi: 10.1074/jbc.273.1.215.

Arimura, Akira, Aniko Somogyvári-Vigh, Atsuro Miyata, Keiko Mizuno, David H. Coy, and Chieko Kitada. 1991. "Tissue Distribution of PACAP as Determined by RIA: Highly Abundant in the Rat Brain and Testes." *Endocrinology* 129(5):2787–89. doi: 10.1210/endo-129-5-2787.

Arisawa, Kotoko, Ayumi Matsuoka, Natsuki Ozawa, Tomoko Ishikawa, Ikuyo Ichi, and Yoko Fujiwara. 2024. "GPER/PKA-Dependent Enhancement of Hormone-Sensitive Lipase Phosphorylation in 3T3-L1 Adipocytes by Piceatannol." *Nutrients* 16(1):1–12. doi: 10.3390/nu16010038.

Beaudet, Matthew M., Karen M. Braas, and Victor May. 1998. "Pituitary Adenylate Cyclase-Activating Polypeptide (PACAP) Expression in Sympathetic Preganglionic Projection Neurons to the Superior Cervical Ganglion." *Journal of Neurobiology* 36(3):325–36. doi: 10.1002/(SICI)1097-4695(19980905)36:3<325::AID-NEU2>3.0.CO;2-Y.

Belfrage, Per, Eva Degerman, Cecilia Holm, Dominique Langin, Vincent Manganiello. 1997. "Regulation of Hormone-Sensitive Lipase Activity in Adipose Tissue." *Methods in Enzymology* 286(1988):45–67. doi: 10.1016/S0076-6879(97)86004-1.

Boehm, Stefan, and Sigismund Huck. 1997. "Receptors Controlling Transmitter Release from Sympathetic Neurons *In Vitro*." *Progress in Neurobiology* 51(3):225–42. doi: 10.1016/S0301-0082(96)00056-1.

Braas, Karen M., and Victor May. 1999. "Pituitary Adenylate Cyclase-Activating Polypeptides Directly Stimulate Sympathetic Neuron Neuropeptide Y Release Through PAC1 Receptor Isoform Activation of Specific Intracellular Signaling Pathways." *Journal of Biological Chemistry* 274(39):27702–10. doi: 10.1074/jbc.274.39.27702.

Bray, George A. 2004. "Medical Consequences of Obesity." *Journal of Clinical Endocrinology and Metabolism* 89(6):2583–89. doi: 10.1210/jc.2004-0535.

Campbell-Scherer, Denise, and Arya Mitra Sharma. 2016. “Improving Obesity Prevention and Management in Primary Care in Canada.” *Current Obesity Reports* 5(3):327–32. doi: 10.1007/s13679-016-0222-y.

Cannon, Barbara, and Jan Nedergaard. 2004. “Brown Adipose Tissue: Function and Physiological Significance.” *Physiological Reviews* 84(1):277–359. doi: 10.1152/physrev.00015.2003.

Cero, Cheryl, Hannah J. Lea, Kenneth Y. Zhu, and Aaron M. Cypess. 2020. “2020-P: β3-Adrenergic Receptors Regulate Lipolysis and Thermogenesis in Human Brown/Beige Adipocytes.” *Diabetes* 69(Supplement_1):1–20. doi: 10.2337/db20-2020-p.

Charan, Jaykaran, and N. Kantharia. 2013. “How to Calculate Sample Size in Animal Studies?” *Journal of Pharmacology and Pharmacotherapeutics* 4(4):303–6. doi: 10.4103/0976-500X.119726.

Chen, Kong Y., Robert J. Brychta, Zahraa Abdul Sater, Thomas M. Cassimatis, Cheryl Cero, Laura A. Fletcher, Nikita S. Israni, James W. Johnson, Hannah J. Lea, Joyce D. Linderman, Alana E. O’Mara, Kenneth Y. Zhu, and Aaron M. Cypess. 2020. “Opportunities and Challenges in the Therapeutic Activation of Human Energy Expenditure and Thermogenesis to Manage Obesity.” *Journal of Biological Chemistry* 295(7):1926–42. doi: 10.1074/jbc.REV119.007363.

Chooi, Yu Chung, Cherlyn Ding, and Faidon Magkos. 2019. “The Epidemiology of Obesity.” *Metabolism: Clinical and Experimental* 92:6–10. doi: 10.1016/j.metabol.2018.09.005.

Cinti, Saverio. 2005. “The Adipose Organ.” *Prostaglandins Leukotrienes and Essential Fatty Acids* 73(1 SPEC. ISS.):9–15. doi: 10.1016/j.plefa.2005.04.010.

Clemmensen, Christoffer, Sigrid Jall, Maximilian Kleinert, Carmelo Quarta, Tim Gruber, Josefine Reber, Stephan Sachs, Katrin Fischer, Annette Feuchtinger, Angelos Karlas, Stephanie E. Simonds, Gerald Grandl, Daniela Loher, Eva Sanchez-Quant, Susanne Keipert, Martin Jastroch, Susanna M. Hofmann, Emmani B. M. Nascimento, Patrick Schrauwen, Vasilis Ntziachristos, Michael A. Cowley, Brian Finan, Timo D. Müller, and Matthias H. Tschöp. 2018. “Coordinated Targeting of Cold and Nicotinic Receptors Synergistically Improves Obesity and Type 2 Diabetes.” *Nature Communications* 9(1). doi: 10.1038/s41467-018-06769-y.

Cline, Daemon L., Landon I. Short, Maeghan A. M. Forster, and Sarah L. Gray. 2019. “Adipose Tissue Expression of PACAP, VIP, and Their Receptors in Response to Cold Stress.” *Journal of Molecular Neuroscience* 68(3):427–38. doi: 10.1007/s12031-018-1099-x.

Couvineau, Alain, and Marc Laburthe. 2012. “VPAC Receptors: Structure, Molecular Pharmacology and Interaction with Accessory Proteins.” *British Journal of*

Pharmacology 166(1):42–50. doi: 10.1111/j.1476-5381.2011.01676.x.

Daniel, Philip B., Timothy J. Kieffer, Colin A. Leech, and Joel F. Habener. 2001. "Novel Alternatively Spliced Exon in the Extracellular Ligand-Binding Domain of the Pituitary Adenylate Cyclase-Activating Polypeptide (PACAP) Type 1 Receptor (PAC1R) Selectively Increases Ligand Affinity and Alters Signal Transduction Coupling During Spermatogenesis." *Journal of Biological Chemistry* 276(16):12938–44. doi: 10.1074/jbc.M009941200.

Dautzenberg, Frank M., G. Mevenkamp, S. Wille, and R. L. Hauger. 1999. "N-Terminal Splice Variants of the Type I PACAP Receptor: Isolation, Characterization and Ligand Binding/Selectivity Determinants." *Journal of Neuroendocrinology* 11(12):941–49. doi: 10.1046/j.1365-2826.1999.00411.x.

Diané, Abdoulaye, Nikolina Nikolic, Alexander P. Rudecki, Shannon M. King, Drew J. Bowie, and Sarah L. Gray. 2014. "PACAP Is Essential for the Adaptive Thermogenic Response of Brown Adipose Tissue to Cold Exposure." *Journal of Endocrinology* 222(3):327–39. doi: 10.1530/JOE-14-0316.

Dickson, Louise, and Keith Finlayson. 2009. "VPAC and PAC Receptors: From Ligands to Function." *Pharmacology and Therapeutics* 121(3):294–316. doi: 10.1016/j.pharmthera.2008.11.006.

Duc, Nguyen Minh, Hee Ryung Kim, and Ka Young Chung. 2015. "Structural Mechanism of G Protein Activation by G Protein-Coupled Receptor." *European Journal of Pharmacology* 763:214–22. doi: 10.1016/j.ejphar.2015.05.016.

Duncan, Robin E., Maryam Ahmadian, Kathy Jaworski, Eszter Sarkadi-Nagy, and Hei Sook Sul. 2007. "Regulation of Lipolysis in Adipocytes." *Annual Review of Nutrition* 27:79–101. doi: 10.1146/annurev.nutr.27.061406.093734.

Eiden, Lee E., Andrew C. Emery, Limei Zhang, and Corey B. Smith. 2018. "PACAP Signaling in Stress: Insights from the Chromaffin Cell." *Pflugers Archiv European Journal of Physiology* 470(1):79–88. doi: 10.1007/s00424-017-2062-3.

Eisenhofer, Graeme, Irwin J. Kopin, and David S. Goldstein. 2004. "Catecholamine Metabolism: A Contemporary View with Implications for Physiology and Medicine." *Pharmacological Reviews* 56(3):331–49. doi: 10.1124/pr.56.3.1.

Esteve, Eduardo, Wifredo Ricart, and José Manuel Fernández-Real. 2009. "Adipocytokines and Insulin Resistance: The Possible Role of Lipocalin-2, Retinol Binding Protein-4, and Adiponectin." *Diabetes Care* 32 Suppl 2. doi: 10.2337/dc09-s340.

Filatov, Ekaterina, Landon I. Short, Maeghan A. M. Forster, Simon S. Harris, Erik N. Schien, Malcolm C. Hughes, Daemon L. Cline, Colin J. Appleby, and Sarah L. Gray. 2021. "Contribution of Thermogenic Mechanisms by Male and Female Mice Lacking Pituitary

Adenylate Cyclase-Activating Polypeptide in Response to Cold Acclimation." *American Journal of Physiology - Endocrinology and Metabolism* 320(3):475–87. doi: 10.1152/AJPENDO.00205.2020.

François, Marie, Hayden Torres, Clara Huesing, Rui Zhang, Carson Saurage, Nathan Lee, Emily Qualls-creekmore, Sangho Yu, Christopher D. Morrison, David Burk, Hans Rudolf Berthoud, and Heike Münzberg. 2019. "Sympathetic Innervation of the Interscapular Brown Adipose Tissue in Mouse." 1–11. doi: 10.1111/nyas.14119.

Funcke, Jan Bernd, and Philipp E. Scherer. 2019. "Beyond Adiponectin and Leptin: Adipose Tissue-Derived Mediators of Inter-Organ Communication." *Journal of Lipid Research* 60(10):1648–97. doi: 10.1194/jlr.R094060.

Garton, Andrew J., David G. Campbell, Philip Cohen, and Stephen J. Yeaman. 1988. "Primary Structure of the Site on Bovine Hormone-Sensitive Lipase Phosphorylated by Cyclic AMP-Dependent Protein Kinase." *FEBS Letters* 229(1):68–72. doi: 10.1016/0014-5793(88)80799-3.

Goldstein and Kopin, Irwin J. 2018. "Adrenomedullary, Adrenocortical, and Sympathoneural Responses to Stressors: A Meta-analysis." *Physiology & Behavior* 176(5):139–48. PMID: 18999898.

Goldstein, David S. 2021. "Stress and the 'Extended' Autonomic System." *Autonomic Neuroscience: Basic and Clinical* 236(June):102889. doi: 10.1016/j.autneu.2021.102889.

Gray Henry. 2008. Gray's Anatomy: The classic 1860 edition with original illustrations by henry carter. London, UK: Arcturus Publishing Limited.

Gray, Sarah L., and Daemon L. Cline. 2019. "PACAP: Regulator of the Stress Response." *Stress: Physiology, Biochemistry, and Pathology* 3(2019):279-291. doi: 10.1016/B978-0-12-813146-6.00021-7.

Gray, Sarah L., Kevin J. Cummings, Frank R. Jirik, and Nancy M. Sherwood. 2001. "Targeted Disruption of the Pituitary Adenylate Cyclase-Activating Polypeptide Gene Results in Early Postnatal Death Associated with Dysfunction of Lipid and Carbohydrate Metabolism." *Molecular Endocrinology* 15(10):1739–47. doi: 10.1210/mend.15.10.0705.

Gray, Sarah L., Nobuharu Yamaguchi, Petra Vencová, and Nancy M. Sherwood. 2002. "Temperature-Sensitive Phenotype in Mice Lacking Pituitary Adenylate Cyclase-Activating Polypeptide." *Endocrinology* 143(10):3946–54. doi: 10.1210/en.2002-220401.

Haass, Markus, and Wolfgang Kübler. 1997. "Nicotine and Sympathetic Neurotransmission." *Cardiovascular Drugs and Therapy* 10(6):657–65. doi: 10.1007/BF00053022.

Hamelink, Carol, Olga Tjurmina, Ruslan Damadzic, W. Scott Young, Eberhard Weihe, Hyeon Woo Lee, and Lee E. Eiden. 2002. "Pituitary Adenylate Cyclase-Activating Polypeptide Is a Sympathoadrenal Neurotransmitter Involved in Catecholamine Regulation and Glucohomeostasis." *Proceedings of the National Academy of Sciences of the United States of America* 99(1):461–66. doi: 10.1073/pnas.012608999.

Harada, Kenji, Wen Jun Shen, Shailja Patel, Vanita Natu, Jining Wang, Jun Ichi Osuga, Shun Ishibashi, and Fredric B. Kraemer. 2003. "Resistance to High-Fat Diet-Induced Obesity and Altered Expression of Adipose-Specific Genes in HSL-Deficient Mice." *American Journal of Physiology - Endocrinology and Metabolism* 285(6 48-6):1182–95. doi: 10.1152/ajpendo.00259.2003.

Harmar, Anthony J., Jan Fahrenkrug, Illana Gozes, Marc Laburthe, Victor May, Joseph R. Pisegna, David Vaudry, Hubert Vaudry, James A. Waschek, and Sami I. Said. 2012. "Pharmacology and Functions of Receptors for Vasoactive Intestinal Peptide and Pituitary Adenylate Cyclase-Activating Polypeptide: IUPHAR Review 1." *British Journal of Pharmacology* 166(1):4–17. doi: 10.1111/j.1476-5381.2012.01871.x.

Harms, Matthew, and Patrick Seale. 2013. "Brown and Beige Fat: Development, Function and Therapeutic Potential." *Nature Medicine* 19(10):1252–63. doi: 10.1038/nm.3361.

Hashimoto, Hitoshi, Norihito Shintani, Mamoru Tanida, Atsuko Hayata, Ryota Hashimoto, and Akemichi Baba. 2011. "PACAP Is Implicated in the Stress Axes." *Current Pharmaceutical Design* 17(10):985–89. doi: 10.2174/138161211795589382.

Hogg, Ron C., Mario Raggenbass, and Daniel Bertrand. 2003. "Nicotinic Acetylcholine Receptors: From Structure to Brain Function." *Reviews of Physiology, Biochemistry and Pharmacology* 147(March):1–46. doi: 10.1007/s10254-003-0005-1.

Horwitz, Joel, and Robert L. Perlman. 1984. "Activation of Tyrosine Hydroxylase in the Superior Cervical Ganglion by Nicotinic and Muscarinic Agonists." *Journal of Neurochemistry* 43(2):546–52. doi: 10.1111/j.1471-4159.1984.tb00933.x.

Howell, David C. 2013. Statistical Methods for Psychology*,* Eighth Edition. Wadsworth, Cengage Learning, Pages 231-247.

Kandel, Eric R., James H. Schwartz, Thomas M. Jessell, Steven A. Siegelbaum. 2021. Principles of Neural Science*,* Sixth Edition. McGraw Hill. Vol. 01.

Kao, Shih Chu, Rama K. Jaiswal, Walter Kolch, and Gary E. Landreth. 2001. "Identification of the Mechanisms Regulating the Differential Activation of the MAPK Cascade by Epidermal Growth Factor and Nerve Growth Factor in PC12 Cells." *Journal of Biological Chemistry* 276(21):18169–77. doi: 10.1074/jbc.M008870200.

Kazak, Lawrence, Edward T. Chouchani, Mark P. Jedrychowski, Brian K. Erickson, Kosaku

Shinoda, Paul Cohen, Ramalingam Vetrivelan, Gina Z. Lu, Dina Laznik-Bogoslavski, Sebastian C. Hasenfuss, Shingo Kajimura, Steve P. Gygi, and Bruce M. Spiegelman. 2015. “A Creatine-Driven Substrate Cycle Enhances Energy Expenditure and Thermogenesis in Beige Fat.” *Cell* 163(3):643–55. doi: 10.1016/j.cell.2015.09.035.

Kgedal, Bertil, and David S. Goldstein. 1988. “Catecholamines and Their Metabolites.” *Journal of Chromatography B: Biomedical Sciences and Applications* 429(C):177–233. doi: 10.1016/S0378-4347(00)83871-2.

Kooijman, Sander, José K. van den Heuvel, and Patrick C. N. Rensen. 2015. “Neuronal Control of Brown Fat Activity.” *Trends in Endocrinology and Metabolism* 26(11):657–68. doi: 10.1016/j.tem.2015.09.008.

Kraemer, Fredric B., Sinal Patel, Mohammad S. Saedi, and Carole Sztalryd. 1993. “Detection of Hormone-Sensitive Lipase in Various Tissues. I. Expression of an HSL/Bacterial Fusion Protein and Generation of Anti-HSL Antibodies.” *Journal of Lipid Research* 34(4):663–71. doi: 10.1016/s0022-2275(20)39990-9.

Kuri, Barbara A., Shyue An Chan, and Corey B. Smith. 2009. “PACAP Regulates Immediate Catecholamine Release from Adrenal Chromaffin Cells in an Activity-Dependent Manner through a Protein Kinase C-Dependent Pathway.” *Journal of Neurochemistry* 110(4):1214–25. doi: 10.1111/j.1471-4159.2009.06206.x.

Lass, Achim, Robert Zimmermann, Monika Oberer, and Rudolf Zechner. 2011. “Lipolysis - A Highly Regulated Multi-Enzyme Complex Mediates the Catabolism of Cellular Fat Stores.” *Progress in Lipid Research* 50(1):14–27. doi: 10.1016/j.plipres.2010.10.004.

Lehmann, Michael L., Tomris Mustafa, Adrian M. Eiden, Miles Herkenham, and Lee E. Eiden. 2013. “PACAP-Deficient Mice Show Attenuated Corticosterone Secretion and Fail to Develop Depressive Behavior during Chronic Social Defeat Stress.” *Psychoneuroendocrinology* 38(5):702–15. doi: 10.1016/j.psyneuen.2012.09.006.

Leyton, Julius, Ychoshua Gozes, Joseph Pisegna, David Coy, Sally Purdom, Marchessini Casibang, Farah Zia, and Terry W. Moody. 1999. “PACAP(6-38) Is a PACAP Receptor Antagonist for Breast Cancer Cells.” *Breast Cancer Research and Treatment* 56(2):177–86. doi: 10.1023/a:1006262611290.

Livett, Bruce G., Vladimir Kozousek, Fumio Mizobe, and Deanne M. Dean. 1979. “Substance P Inhibits Nicotinic Activation of Chromaffin Cells.” *Nature* 278(5701):256–57. doi: 10.1038/278256A0.

Lupien, John R., and George A. Bray. 1988. “Nicotine Increases Thermogenesis in Brown Adipose Tissue in Rats.” *Pharmacology, Biochemistry and Behavior* 29(1):33–37. doi: 10.1016/0091-3057(88)90269-9.

Lymperopoulos, Anastasios, Ava Brill, and Katie A. McCrink. 2016. “GPCRs of Adrenal

Chromaffin Cells & Catecholamines: The Plot Thickens." *International Journal of Biochemistry and Cell Biology* 77(2016):213–19. doi: 10.1016/j.biocel.2016.02.003.

Mackay, Angus V.P., Iversen, Leslie L. 1972. "Trans-Synaptic Regulation of Tyrosine Hydroxylase Activity in Adrenergic Neurones: Effect of Potassium Concentration on Cultured Sympathetic Ganglia." *The Biochemical Journal* 128(3):225–29. doi: 10.1042/bj1280083P.

May, Victor, Cynthia A. Brandenburg, and Karen M. Braas. 1995. "Differential Regulation of Sympathetic Neuron Neuropeptide Y and Catecholamine Content and Secretion." *Journal of Neuroscience* 15(6):4580–91. doi: 10.1523/jneurosci.15-06-04580.1995.

Miyata, Atsuro, Akira Arimura, Raymond R. Dahl, Naoto Minamino, Akira Uehara, Lun Jiang, Michael D. Culler, and David H. Coy. 1989. "Isolation of a Novel 38 Residue-Hypothalamic Polypeptide Which Stimulates Adenylate Cyclase in Pituitary Cells." *Biochemical and Biophysical Research Communications* 164(1):567–74. doi: 10.1016/0006-291X(89)91757-9.

Mizobe, Fumio, and Bruce G. Livett. 1983. "Nicotine Stimulates Secretion of Both Catecholamines and Acetylcholinesterase from Cultured Adrenal Chromaffin Cells." *Journal of Neuroscience* 3(4):871–76. doi: 10.1523/jneurosci.03-04-00871.1983.

Moro, Osamu, and Ethan A. Lerner. 1997. "Maxadilan, the Vasodilator from Sand Flies, Is a Specific Pituitary Adenylate Cyclase-Activating Peptide Type I Receptor Agonist." *Journal of Biological Chemistry* 272(2):966–70. doi: 10.1074/jbc.272.2.966.

Mustafa, Tomris. 2013. "Pituitary Adenylate Cyclase-Activating Polypeptide (PACAP). A Master Regulator in Central and Peripheral Stress Responses." *Advances in Pharmacology* 68(2013):445-457. doi: 10.1016/B978-0-12-411512-5.00021-X.

Nedergaard, Jan, Stefan Alexson, and Barbara Cannon. 1980. "Cold Adaptation in the Rat: Increased Brown Fat Peroxisomal β-Oxidation Relative to Maximal Mitochondrial Oxidative Capacity." *American Journal of Physiology - Cell Physiology* 8(3). doi: 10.1152/ajpcell.1980.239.5.c208.

Pan, Warren W., and Martin G. Myers. 2018. "Leptin and the Maintenance of Elevated Body Weight." *Nature Reviews Neuroscience* 19(2):95–105. doi: 10.1038/nrn.2017.168.

Pandher, Parleen K., Yamna Rahim, Katherine P. Timms, Ekaterina Filatov, Landon I. Short, and Sarah L. Gray. 2023. "Reference Gene Recommendations and PACAP Receptor Expression in Murine Sympathetic Ganglia of the Autonomic Nervous System That Innervate Adipose Tissues after Chronic Cold Exposure." *Journal of Neuroendocrinology* 35(8):1–12. doi: 10.1111/jne.13313.

Pantaloni, Colette, Philippe Brabet, Benoit Bilanges, Aline Dumuis, Souheir Houssami, Dietmar Spengler, Joël Bockaert, and Laurent Journot. 1996. "Alternative Splicing in

the N-Terminal Extracellular Domain of the Pituitary Adenylate Cyclase-Activating Polypeptide (PACAP) Receptor Modulates Receptor Selectivity and Relative Potencies of PACAP-27 and PACAP-38 in Phospholipase C Activation." *Journal of Biological Chemistry* 271(36):22146–51. doi: 10.1074/jbc.271.36.22146.

Percie du Sert, Nathalie, Viki Hurst, Amrita Ahluwalia, Sabina Alam, Marc T. Avey, Monya Baker, William J. Browne, Alejandra Clark, Innes C. Cuthill, Ulrich Dirnagl, Michael Emerson, Paul Garner, Stephen T. Holgate, David W. Howells, Natasha A. Karp, Stanley E. Lazic, Katie Lidster, Catriona J. MacCallum, Malcolm Macleod, Esther J. Pearl, Ole H. Petersen, Frances Rawle, Penny Reynolds, Kieron Rooney, Emily S. Sena, Shai D. Silberberg, Thomas Steckler, and Hanno Würbel. 2020. "The ARRIVE Guidelines 2.0: Updated Guidelines for Reporting Animal Research." *British Journal of Pharmacology* 177(16):3617–24. doi: 10.1111/bph.15193.

Pinto, Renata Machado, Cristiane Cominetti, and Aparecido Divino da Cruz. 2016. "Basic and Genetic Aspects of Food Intake Control and Obesity: Role of Dopamin Receptor D2 TaqIA Polymorphism." *Obesity Research - Open Journal* 2(4):119–27.

Resch, Jon M., Joanne P. Boisvert, Allison E. Hourigan, Christopher R. Mueller, Sun Shin Yi, and Sujean Choi. 2011. "Stimulation of the Hypothalamic Ventromedial Nuclei by Pituitary Adenylate Cyclase-Activating Polypeptide Induces Hypophagia and Thermogenesis." *American Journal of Physiology - Regulatory Integrative and Comparative Physiology* 301(6):1625–34. doi: 10.1152/ajpregu.00334.2011.

Rhoades, Rodney A., David R. Bell. 2013. Medical Physiology: Principles for Clinical Medicine, Fourth Edition. Wolters Kluwer Health/Lippincott Williams & Wilkins.

Rosenwald, Matthias, Aliki Perdikari, Thomas Rülicke, and Christian Wolfrum. 2013. "Bi-Directional Interconversion of Brite and White Adipocytes." *Nature Cell Biology* 15(6):659–67. doi: 10.1038/ncb2740.

Rothman, Kenneth J. 2008. "BMI-Related Errors in the Measurement of Obesity." *International Journal of Obesity* 32:S56–59. doi: 10.1038/ijo.2008.87.

Sakers, Alexander, Mirian Krystel De Siqueira, Patrick Seale, and Claudio J. Villanueva. 2022. "Adipose-Tissue Plasticity in Health and Disease." *Cell* 185(3):419–46. doi: 10.1016/j.cell.2021.12.016.

du Sert, Nathalie Percie, Amrita Ahluwalia, Sabina Alam, Marc T. Avey, Monya Baker, William J. Browne, Alejandra Clark, Innes C. Cuthill, Ulrich Dirnagl, Michael Emerson, Paul Garner, Stephen T. Holgate, David W. Howells, Viki Hurst, Natasha A. Karp, Stanley E. Lazic, Katie Lidster, Catriona J. MacCallum, Malcolm Macleod, Esther J. Pearl, Ole H. Petersen, Frances Rawle, Penny Reynolds, Kieron Rooney, Emily S. Sena, Shai D. Silberberg, Thomas Steckler, and Hanno Würbel. 2020. "Reporting Animal Research: Explanation and Elaboration for the Arrive Guidelines 2.0." *PLoS Biol* 18(7):e3000411.Vol. 18. doi: 10.1371/journal.pbio.3000411.

Sherwood, Nancy M., Sandra L. Krueckl, and John E. Mcrory. 2000. “The Origin and Function of the Pituitary Adenylate Cyclase-Activating Polypeptide (PACAP)/Glucagon Superfamily.” *Endocrine Reviews* 21(6):619–70. doi: 10.1210/edrv.21.6.0414.

Smith, Kristy Breuhl, and Michael Seth Smith. 2016. “Obesity Statistics.” *Primary Care - Clinics in Office Practice* 43(1):121–35. doi: 10.1016/j.pop.2015.10.001.

Spiegelman, Bruce M., and Jeffrey S. Flier. 2001. “Obesity and the Regulation of Energy Balance.” *Cell* 104:531–43. doi: 10.1016/S0092-8674(01)00240-9.

Spongier, Dietmar, Christian Waeber, Colette Pantaloni, Florian Holsboer, Joël Bockaert, Peter H. Seeburgt, and Laurent Journot. 1993. “Differential Signal Transduction by Five Splice Variants of the PACAP Receptor.” *Nature* 365(6442):170–75. doi: 10.1038/365170a0.

Stroth, Nikolas, Barbara A. Kuri, Tomris Mustafa, Shyue A. Chan, Corey B. Smith, and Lee E. Eiden. 2013. “PACAP Controls Adrenomedullary Catecholamine Secretion and Expression of Catecholamine Biosynthetic Enzymes at High Splanchnic Nerve Firing Rates Characteristic of Stress Transduction in Male Mice.” *Endocrinology* 154(1):330–39. doi: 10.1210/en.2012-1829.

Stroth, Nikolas, Yvonne Holighaus, Djida Ait-Ali, and Lee E. Eiden. 2011. “PACAP: A Master Regulator of Neuroendocrine Stress Circuits and the Cellular Stress Response.” *Annals of the New York Academy of Sciences* 1220(1):49–59. doi: 10.1111/j.1749-6632.2011.05904.x.

Susulic, Vedrana S., Robert C. Frederich, Joel Lawitts, Effie Tozzo, Barbara B. Kahn, Mary Ellen Harper, Jean Himms-Hagen, Jeffrey S. Flier, and Bradford B. Lowell. 1995. “Targeted Disruption of the B3-Adrenergic Receptor Gene.” *Journal of Biological Chemistry* 270(49):29483–92. doi: 10.1074/jbc.270.49.29483.

Tanaka, Keiko, Izumi Shibuya, Toshihisa Nagatomo, Hiroshi Yamashita, and Tomio Kanno. 1996. “Pituitary Adenylate Cyclase-Activating Polypeptide Causes Rapid Ca^{2+} Release from Intracellular Stores and Long Lasting Ca^{2+} Influx Mediated by Na^{+} Influx-Dependent Membrane Depolarization in Bovine Adrenal Chromaffin Cells.” *Endocrinology* 137(3):956–66. doi: 10.1210/endo.137.3.8603609.

Thesleff, Stephen, and Bernard Katz. 1957. “A Study of the Desensitization Produced by Acetylcholine at the Motor End-Plate.” *Journal of Physiology Paris* 138(1953):63–80. doi: 10.1113/jphysiol.1957.sp005838.

Trendelenburg, Anne Ulrike, Eugen Gerhard Gaiser, Sandra Leagh Cox, Angelika Meyer, and Klaus Starke. 1999. “Mouse Postganglionic Sympathetic Neurons: Primary Culturing and Noradrenaline Release.” *Journal of Neurochemistry* 73(4):1431–38. doi: 10.1046/j.1471-4159.1999.0731431.x.

Uchida, Daigaku, Ichiro Tatsuno, Tomoaki Tanaka, Aizan Hirai, Yoshifuru Saito, Osamu Moro, and Masahiro Tajima. 1998. "Maxadilan Is a Specific Agonist and Its Deleted Peptide (M65) Is a Specific Antagonist for PACAP Type 1 Receptor." *Annals of the New York Academy of Sciences* 865:253–58. doi: 10.1111/j.1749-6632.1998.tb11185.x.

Ulrich-Lai, Yvonne M., and James P. Herman. 2009. "Neural Regulation of Endocrine and Autonomic Stress Responses." *Nature Reviews Neuroscience* 10(6):397–409. doi: 10.1038/nrn2647.

Upadhyay, Jagriti, Olivia Farr, Nikolaos Perakakis, Wael Ghaly, and Christos Mantzoros. 2018. "Obesity as a Disease." *Medical Clinics of North America* 102(1):13–33. doi: 10.1016/j.mcna.2017.08.004.

Vaudry, David, Anthony Falluel-Morel, Steve Bourgault, Magali Basille, Delphine Burel, Olivier Wurtz, Alain Fournier, Billy K. C. Chow, Hitoshi Hashimoto, Ludovic Galas, and Hubert Vaudry. 2009. "Pituitary Adenylate Cyclase-Activating Polypeptide and Its Receptors: 20 Years after the Discovery." *Pharmacological Reviews* 61(3):283–357. doi: 10.1124/pr.109.001370.

Vaughan, Cheryl H., Eleen Zarebidaki, J. Christopher Ehlen, Timothy J. Bartness. 2014. "Analysis and Measurement of the Sympathetic and Sensory Innervation of White and Brown Adipose Tissue." *Bone* 23(1):1–7. doi: 10.1016/B978-0-12-411619-1.00011-2.

Wu, Jun, Pontus Boström, Lauren M. Sparks, Li Ye, Jang Hyun Choi, An Hoa Giang, Melin Khandekar, Kirsi A. Virtanen, Pirjo Nuutila, Gert Schaart, Kexin Huang, Hua Tu, Wouter D. Van Marken Lichtenbelt, Joris Hoeks, Sven Enerbäck, Patrick Schrauwen, and Bruce M. Spiegelman. 2012. "Beige Adipocytes Are a Distinct Type of Thermogenic Fat Cell in Mouse and Human." *Cell* 150(2):366–76. doi: 10.1016/j.cell.2012.05.016.

Yoshimura, M. Cooper, Laurent Journot, Christian Waeber, Colette Pantaloni, Florian Holsboert, Peter H. Seeburgt, Joël Bockaert, and Dietmar Spenglert. 1995. "Differential Signal Transduction by Six Splice Variants of the Pituitary Adenylate Cyclase-Activating Peptide (PACAP) Receptor." *J. Biol. Chem. Proc. Natl. Acad. Sci. U.S.A* 23(1):133–37. doi: 10.1042/bst0230133.

Zaveri, Nurulain, Faming Jiang, Cris Olsen, Willma Polgar, and Lawrence Toll. 2010. "Novel A3β4 Nicotinic Acetylcholine Receptor-Selective Ligands. Discovery, Structure-Activity Studies, and Pharmacological Evaluation." *Journal of Medicinal Chemistry* 53(22):8187–91. doi: 10.1021/jm1006148.

Zhu, Qi, Xian Liu, Bradley J. Glazier, Kristen N. Krolick, Shangyuwen Yang, Jingyan He, Chunmin C. Lo, and Haifei Shi. 2019. "Differential Sympathetic Activation of Adipose Tissues by Brain-Derived Neurotrophic Factor." *Biomolecules* 9(9). doi: 10.3390/biom9090452.

APPENDIX

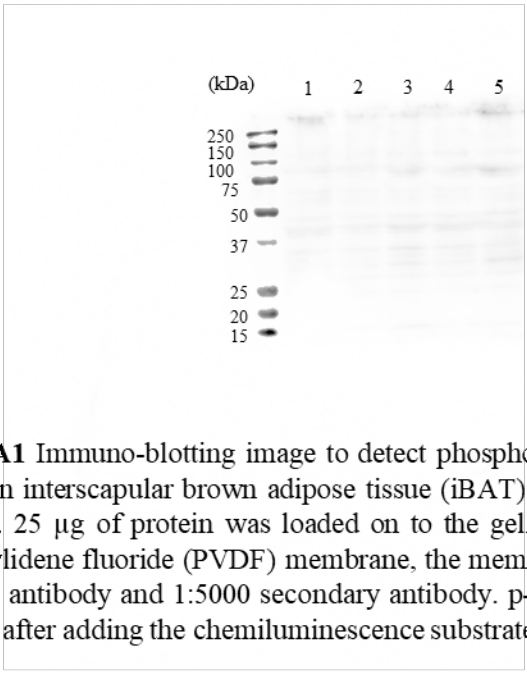

Figure A1 Immuno-blotting image to detect phospho-hormone-sensitive lipase (p-HSL) (Ser660) protein in interscapular brown adipose tissue (iBAT) (n=5) used to optimize the Western blotting protocol. 25 µg of protein was loaded on to the gel, proteins were transferred from the gel to a polyvinylidene fluoride (PVDF) membrane, the membrane was incubated with 1:5000 anti-p-HSL (Ser660) antibody and 1:5000 secondary antibody. p-HSL (Ser660) (83 kD) protein band was not detected after adding the chemiluminescence substrate.

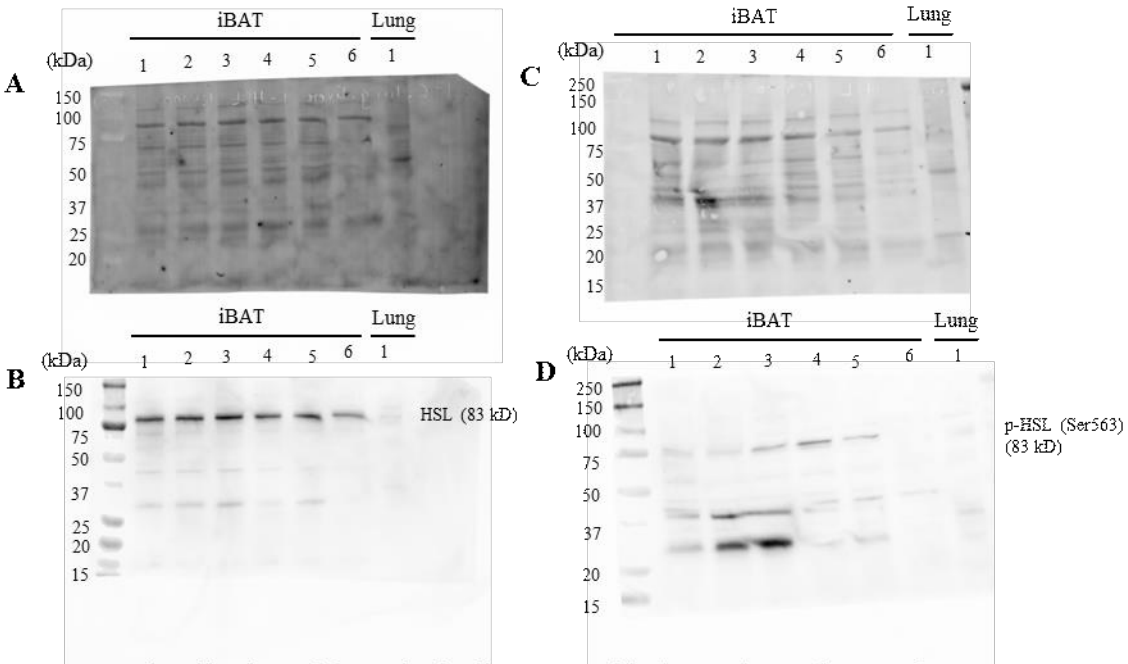

Figure A2 Visualization of the polyvinylidene fluoride (PVDF) membrane after protein transfer to detect total protein (100 to 37 kD) (**A**) used to normalize the expression of hormone-sensitive lipase (HSL) (83 kD) (**B**) detected after adding the chemiluminescence substrate. Similarly, the PVDF membrane for the phospho-HSL (p-HSL) (Ser563) protein was visualized after protein transfer to detect total protein (100 to 37 kD) (**C**) used to normalize the expression of p-HSL (Ser563) (83 kD) (**D**).

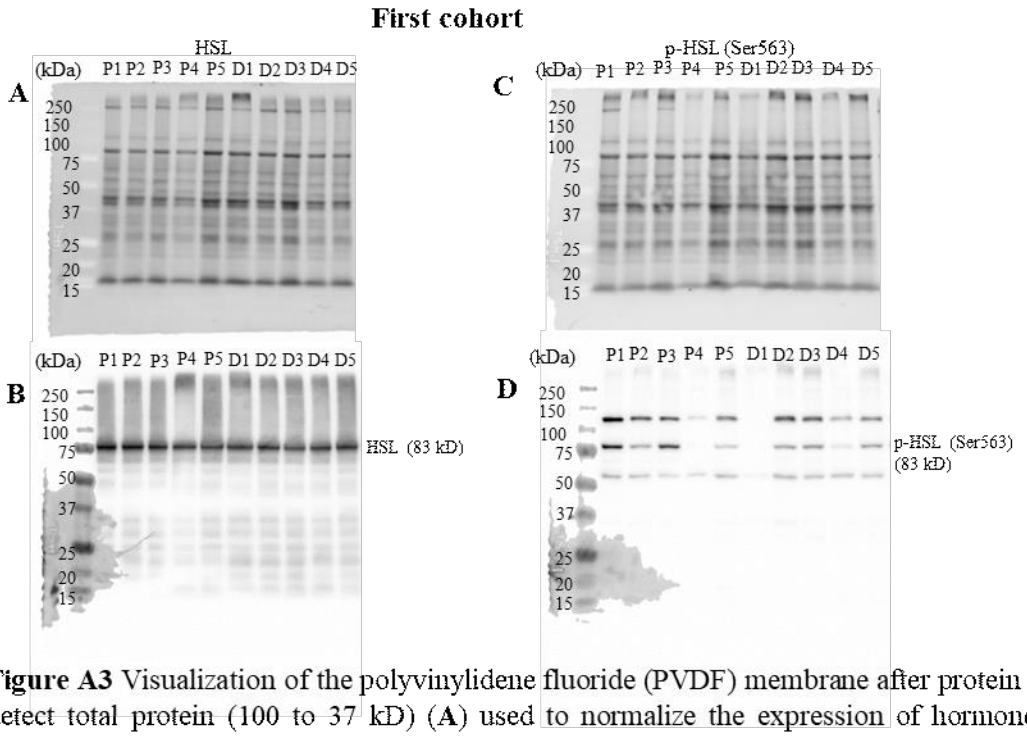

Figure A3 Visualization of the polyvinylidene fluoride (PVDF) membrane after protein transfer to detect total protein (100 to 37 kD) (**A**) used to normalize the expression of hormone-sensitive lipase (HSL) (83 kD) (**B**) detected after adding the chemiluminescence substrate. Similarly, the PVDF membrane for the phospho-HSL (p-HSL) (Ser563) protein was visualized after protein transfer to detect total protein (100 to 37 kD) (**C**) used to normalize the expression of p-HSL (Ser563) (83 kD) (**D**). P1 to P5 are PBS-treated samples and D1 to D5 are DMPP-treated samples from the first cohort.

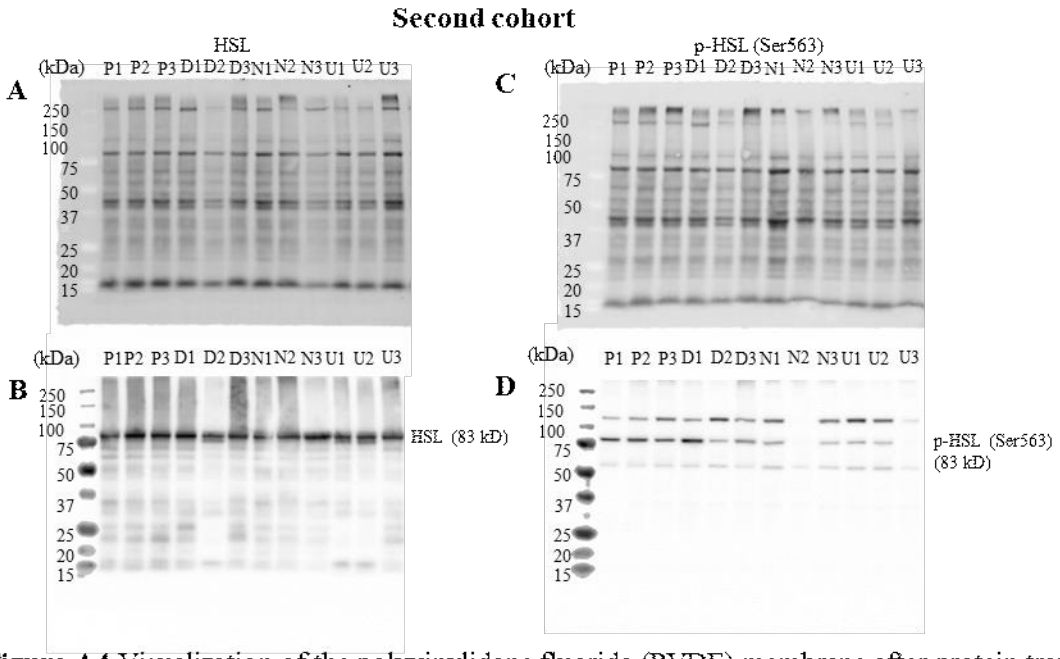

Figure A4 Visualization of the polyvinylidene fluoride (PVDF) membrane after protein transfer to detect total protein (100 to 37 kD) (**A**) used to normalize the expression of hormone-sensitive lipase (HSL) (83 kD) (**B**) detected after adding the chemiluminescence substrate. Similarly, the PVDF membrane for the phospho-HSL (p-HSL) (Ser563) protein was visualized after protein transfer to detect total protein (100 to 37 kD) (**C**) used to normalize the expression of p-HSL (Ser563) (83 kD) (**D**). P1 to P3 are PBS-treated samples, D1 to D3 are DMPP-treated samples, N1 to N3 are nicotine-treated samples, and U1 to U3 are untreated samples from the second cohort.

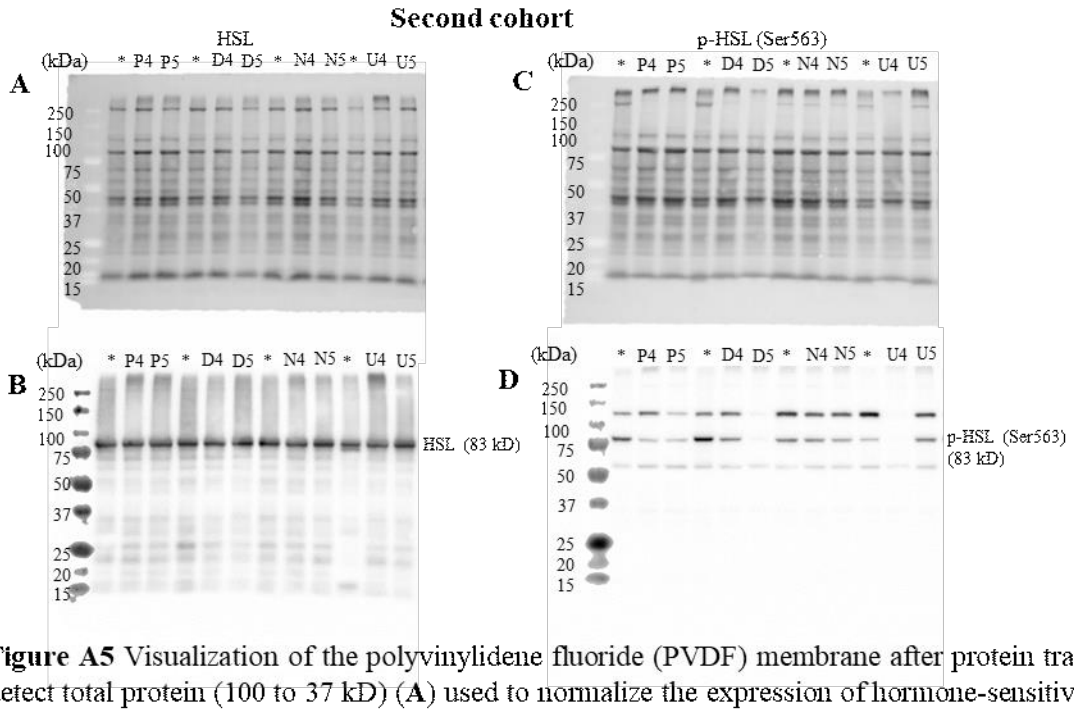

Figure A5 Visualization of the polyvinylidene fluoride (PVDF) membrane after protein transfer to detect total protein (100 to 37 kD) (**A**) used to normalize the expression of hormone-sensitive lipase (HSL) (83 kD) (**B**) detected after adding the chemiluminescence substrate. Similarly, the PVDF membrane for the phospho-HSL (p-HSL) (Ser563) protein was visualized after protein transfer to detect total protein (100 to 37 kD) (**C**) used to normalize the expression of p-HSL (Ser563) (83 kD) (**D**). P4 and P5 are PBS-treated samples, D4 and D5 are DMPP-treated samples, N4 and N5 are nicotine-treated samples, U4 and U5 are untreated samples from the second cohort. Asterisks (*) denotes the inter-gel calibrators (the first sample from each group).

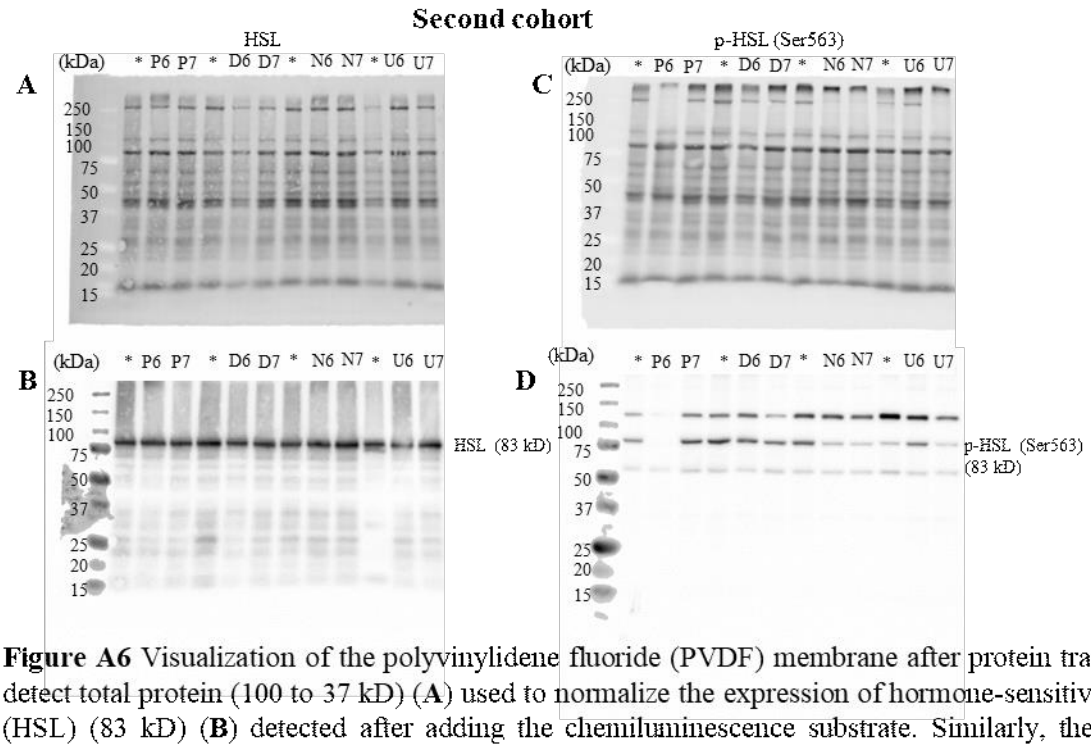

Figure A6 Visualization of the polyvinylidene fluoride (PVDF) membrane after protein transfer to detect total protein (100 to 37 kD) (**A**) used to normalize the expression of hormone-sensitive lipase (HSL) (83 kD) (**B**) detected after adding the chemiluminescence substrate. Similarly, the PVDF membrane for the phospho-HSL (p-HSL) (Ser563) protein was visualized after protein transfer to detect total protein (100 to 37 kD) (**C**) used to normalize the expression of p-HSL (Ser563) (83 kD) (**D**). P6 and P7 are PBS-treated samples, D6 and D7 are DMPP-treated samples, N6 and N7 are nicotine-treated samples, U6 and U7 are untreated samples from the second cohort. Asterisks (*) denotes the inter-gel calibrators (the first sample from each group).